



RESEARCH ARTICLE

10.1029/2021MS002760

Evaluation of Secondary Organic Aerosol (SOA) Simulations for Seoul, Korea

Key Points:

- Model evaluation of simulated organic aerosols (OA) using different secondary organic aerosols (SOA) schemes in Seoul shows large variability
- The inclusion of semi/intermediate volatile precursors and chemical aging are important factors in reducing model biases
- The simplified SOA scheme can reproduce observed OA, but uncertainties exist in precursor parameterization in Seoul

Supporting Information:

Supporting Information may be found in the online version of this article.

Correspondence to:











R. J. Park,
rjpark@snu.ac.kr

Citation:

Oak, Y. J., Park, R. J., Jo, D. S., Hodzic, A., Jimenez, J. L., Campuzano-Jost, P., et al. (2022). Evaluation of secondary organic aerosol (SOA) simulations for Seoul, Korea. *Journal of Advances in Modeling Earth Systems*, 14, e2021MS002760. <https://doi.org/10.1029/2021MS002760>

Received 6 AUG 2021

Accepted 20 JAN 2022

Yujin J. Oak¹ , Rokjin J. Park¹ , Duseong S. Jo^{2,3,4} , Alma Hodzic² , Jose L. Jimenez^{3,4} , Pedro Campuzano-Jost^{3,4} , Benjamin A. Nault⁵, Hwajin Kim^{6,7}, Hyeonmin Kim¹, Eunjo S. Ha¹, Chang-Keun Song⁸, Seung-Muk Yi^{9,10}, Glenn S. Diskin¹¹ , Andrew J. Weinheimer² , Donald R. Blake¹² , Armin Wisthaler^{13,14} , Mihee Shim¹⁵, and Yoonmi Shin¹⁵

¹School of Earth and Environmental Sciences, Seoul National University, Seoul, South Korea, ²Atmospheric Chemistry Observations and Modeling Laboratory, National Center for Atmospheric Research, Boulder, CO, USA, ³Cooperative Institute for Research in Environmental Sciences, University of Colorado, Boulder, CO, USA, ⁴Department of Chemistry, University of Colorado, Boulder, CO, USA, ⁵Center for Aerosols and Cloud Chemistry, Aerodyne Research, Inc., Billerica, MA, USA, ⁶Center for Environment, Health and Welfare Research, Korea Institute of Science and Technology, Seoul, South Korea, ⁷Now at Department of Environmental Health, Graduate School of Public Health, Seoul National University, Seoul, South Korea, ⁸School of Urban and Environmental Engineering, Ulsan National Institute of Science and Technology, Ulsan, South Korea, ⁹Department of Environmental Health, Graduate School of Public Health, Seoul National University, Seoul, South Korea, ¹⁰Institute of Health and Environment, Seoul National University, Seoul, South Korea, ¹¹NASA Langley Research Center, Hampton, VA, USA, ¹²Department of Chemistry, University of California at Irvine, Irvine, CA, USA, ¹³Department of Chemistry, University of Oslo, Oslo, Norway, ¹⁴Institute for Ion Physics and Applied Physics, University of Innsbruck, Innsbruck, Austria, ¹⁵Seoul Research Institute of Public Health and Environment, Gwacheon, South Korea

Abstract Organic aerosols (OA) represent a significant fraction of total submicron particulate matter (PM₁) concentrations globally, including densely populated megacities such as Seoul. However, scientific understanding of the atmospheric formation and removal processes of OA, especially for secondary organic aerosols (SOA), is still highly uncertain. In this study, we examine the characteristics of SOA formation in Seoul during spring-summer 2016 and fall-winter 2017/2018, using airborne and ground observations along with a 3-D global chemical transport model, GEOS-Chem. We use four different SOA schemes in the model, including simplified and complex volatility-based frameworks, and evaluate them by comparing the simulations with the observations to examine how our scientific understanding embedded in each SOA scheme affects the observed biases. Our analysis of the model performance of each scheme also provides the most suitable approach in simulating SOA in a typical urban environment. Comparisons of the simulated versus observed OA concentrations show that model biases range from −72% to +118%, with considerable variability among different schemes and seasons. We find that the inclusion of semi/intermediate volatile precursors, in addition to the traditional precursors, and chemical aging (functionalization) are important factors to simulate surface SOA concentrations in Seoul. However, a comparison of observed and simulated SOA/ΔCO enhancement ratios suggests that most schemes underpredict SOA aging in upper levels in the boundary layer. We also find that the simplified SOA scheme can reproduce observed OA but often shows overestimation in surface air, indicating that uncertainties exist in bottom-up emissions and precursor parameterization in Seoul.

Plain Language Summary We compare four different modeling approaches for simulating secondary organic aerosol (SOA) formation, accounting for a significant fraction of total fine particulate matter concentrations in Seoul, Korea. Using GEOS-Chem, a chemical transport model, we find that current SOA schemes show large variabilities. Including an additional precursor species and further oxidation (i.e., chemical aging) of simulated SOA improves model performance. We also find that a simplified scheme with less computational cost can reproduce observed values but generally shows an overestimation in Seoul, indicating uncertainties in parameterization.

1. Introduction

The health effects and climatic impacts of air pollution have been highlighted by several studies (Landrigan et al., 2017; Mukherjee & Agrawal, 2017; Myhre et al., 2013). Many studies focus on the size, distribution, and composition of particulate matter (PM) among the various air pollutants. Understanding the chemical

composition of PM is essential in assessing potential impacts on the atmospheric environment and, therefore, establishing effective regulatory policies.

Observational studies show that organic aerosols (OA) represent a significant fraction (20%–90%) of total sub-micron (diameter $\leq 1 \mu\text{m}$) particulate matter (PM_{10}) concentrations globally (de Gouw & Jimenez, 2009; Zhang et al., 2007; Zhou et al., 2020). A significant amount of OA mass concentration has also been reported in East Asia. For example, in Seoul, a densely populated megacity with a population of ~ 10 million, OA comprises roughly 40% of total non-refractory PM_{10} mass concentrations during late spring (Crawford et al., 2021; Jordan et al., 2020; NIER & NASA, 2017).

Organic species are often directly emitted in the particle phase from anthropogenic and natural combustion sources, known as primary organic aerosols (POA; DeCarlo et al., 2010; Jimenez et al., 2009; Zhang et al., 2007). On the other hand, secondary organic aerosols (SOA) can be formed through heterogeneous and aqueous reactions, and also from the oxidation of precursor gases, called parent hydrocarbons or volatile organic compounds (VOCs), and through the gas-particle partitioning process of oxygenated organic compounds (de Gouw & Jimenez, 2009; Hallquist et al., 2009). Compared to inorganic species that comprise PM, such as sulfate (SO_4^{2-}), nitrate (NO_3^-), and ammonium (NH_4^+) aerosols, scientific understanding of the atmospheric formation and removal processes of OA, especially the atmospheric processing of SOA in urban environments, is still highly uncertain (Hayes et al., 2015). Not only are direct emissions of POA difficult to estimate, but the sources, fates, characterization of precursor species, and the volatility distribution of SOA remain a considerable uncertainty (Hallquist et al., 2009).

Chemical transport models (CTMs) are an effective tool to test the accuracy of emission sources and to investigate the formation and removal processes of OA. Early studies implied that POA, once emitted, remains non-volatile. Thus, models treated POA as a chemically inert species that is only transported or deposited (Bond et al., 2004). However, subsequent studies discovered that POA could act as a semivolatile species, which undergo reversible partitioning, and therefore this process was taken into account in models (Pai et al., 2020; Robinson et al., 2007).

Modeling SOA in CTMs requires both accuracy and simplicity so that the schemes reproduce essential characteristics of the complex processes that lie behind SOA formation. At the same time, they need to be computationally efficient. One of the most traditional SOA modeling schemes is the “two-product approach,” which uses two SOA surrogates that partition at equilibrium based on SOA yields from chamber experiments (Odum et al., 1996). Later, a new approach was introduced to represent continuous oxidation of semivolatile compounds, also known as chemical aging, with the volatility distribution of OA. Donahue et al. (2006) and Stanier et al. (2008) developed the “volatility basis set (VBS) approach,” which divides the wide volatility range into several bins that categorize organic compounds by their volatilities. When subject to aging, their volatilities would change.

Several studies have implemented the VBS approach, accounting for continuous aging within the bins in regional and global models to simulate SOA (Hodzic et al., 2010; Pye & Seinfeld, 2010; Shrivastava et al., 2008). Although recent studies show enhancement in simulated SOA mass, showing improved results compared to the significant model-observation discrepancies that have been reported previously (Tsigaridis et al., 2014), study regions and model resolutions have been limited to a global scale (Hodzic et al., 2016; Jo et al., 2013; Pai et al., 2020). In this study, we examine the characteristics of OA formation in an urban environment, on a finer scale, using airborne and ground observation data along with a global 3-D CTM, GEOS-Chem. Here we compare four SOA schemes, including a simplified approach and three different treatments using the VBS method, and evaluate model performance in Seoul during different seasons in 2016 through 2018. The main objective of this study is to suggest the most suitable approach in representing the observed atmospheric conditions for OA in Seoul.

2. Model Description

We use a 3-D global CTM, GEOS-Chem v12.0.0 (Bey et al., 2001), to simulate OA in East Asia during two different periods, spring-summer 2016 and fall-winter 2017/2018. The model is driven by the Goddard Earth Observing System forward processing (GEOS-FP) assimilated meteorological fields, which have native horizontal resolutions of $0.25^\circ \times 0.3125^\circ$ and hourly to 3-hourly temporal resolutions, provided by the NASA Global Modeling Assimilation Office (GMAO). Global simulations with $2^\circ \times 2.5^\circ$ horizontal resolutions and one-month spin-ups were conducted prior to nested simulations to provide hourly boundary and initial conditions. The nested

Table 1
Monthly Emission Totals of Anthropogenic, Biomass Burning, and Biogenic CO, Secondary Organic Aerosols Precursors, and Primary Organic Carbon in Korea (South)

Emissions [Tg month ⁻¹]	May 2016	July 2016	October 2017	December 2017	February 2018
CO	0.190	0.166	0.141	0.133	0.120
Isoprene	0.030	0.068	0.009	0.000	0.001
Monoterpenes	0.013	0.030	0.007	0.001	0.001
Aromatics	0.031	0.030	0.030	0.029	0.026
S/IVOCs	0.018	0.016	0.014	0.014	0.013
POC	0.005	0.004	0.003	0.003	0.003

configuration covers the East Asian domain (15–55°N, 70–140°E) with $0.25^\circ \times 0.3125^\circ$ horizontal resolution, which corresponds to approximately 30×30 km, and 47 vertical layers using hybrid pressure-sigma coordinates (1013.25–0.010 hPa).

For anthropogenic emissions, including ship emissions, we use the KORUS v5 inventory, which provides monthly emissions of carbon monoxide (CO), nitrogen oxides ($\text{NO}_x = \text{NO} + \text{NO}_2$), sulfur dioxide (SO_2), ammonia (NH_3), speciated VOCs, elemental carbon (EC), and primary organic carbon (POC) in East Asia for 2015–2016 (Jang et al., 2019; Woo et al., 2012). We use the Global Fire Emissions Database 4 (GFED4) inventory for daily biomass burning emissions (van der Werf et al., 2010) and the Model of Emissions of Gases and Aerosols from Nature (MEGAN) v2.1 to calculate online biogenic emissions (Guenther et al., 2012). Emission totals of CO, SOA precursors, and POC in South Korea, including anthropogenic, biomass burning, and biogenic sources for each simulation period, are summarized in Table 1.

Chemical species in GEOS-Chem are simulated using a detailed gas phase tropospheric chemistry mechanism, incorporating hydrogen oxide radicals ($\text{HO}_x = \text{H} + \text{OH} + \text{peroxy radicals}$), NO_x , VOCs, ozone (O_3), and halogens, which is coupled with aerosol simulations that include both secondary inorganic aerosols (SIA; SO_4^{2-} – NO_3^- – NH_4^+) and carbonaceous aerosols (black carbon and organic aerosol). SIA thermodynamics in GEOS-Chem is computed using the ISORROPIA II thermodynamic equilibrium model (Fountoukis & Nenes, 2007). Carbonaceous aerosol simulations include black carbon (BC), referring to the light-absorbing surrogate of EC, which follows the work of Park et al. (2003) and is further described in Wang et al. (2014). GEOS-Chem simulates POC and SOA separately and defines tracers according to their hydrophilicity for POC and volatility for SOA. The model simulates two POC tracers, “OCPO” for hydrophobic POC and “OCPI” for hydrophilic POC, assuming that 50% of POC is emitted from combustion sources as OCPO, which is converted to OCPI with a lifetime of 1.15 days (Cooke et al., 1999; Park et al., 2003). For conversion of POC to POA, we multiply the simulated POC concentrations by an organic aerosol to organic carbon ratio (OA/OC) of 1.3 based on observation-based studies (H. Kim, Zhang, et al., 2017, 2018; Philip et al., 2014). The model assumes an OA/OC ratio of 2.1 to calculate SOA partitioning and simulates SOA tracers as organic matter with molecular weights of 150–250 g mol⁻¹. All unit conversions between mixing ratios and mass densities in the remainder of this study are based on standard temperature and pressure (STP; 273 K and 1013.25 hPa) conditions.

This study compares four different SOA schemes, including the two standard SOA options in GEOS-Chem, the “Complex” and “Simple” schemes, and two additional schemes introduced by Hodzic et al. (2016) and Jo et al. (2013), hereafter referred to as the “Hodzic” and “Jo” schemes. Brief explanations on the main features and updates in each scheme are summarized in Table 2. All schemes, except the Simple scheme, use the VBS approach, which allocates oxygenated organic compounds that are formed by the reactions between oxidants and parent hydrocarbons such as isoprene, terpenes (monoterpenes, sesquiterpenes), aromatics (benzene, toluene, xylene), and semi/intermediate volatile organic compounds (S/IVOCs), into several bins according to their saturation concentrations (C^*).

The Complex SOA scheme builds on the VBS framework implemented by Pye and Seinfeld (2010) with additional updates on isoprene chemistry and SOA formation regarding irreversible uptake to aqueous aerosols (Marais et al., 2016). The volatility-based scheme originally uses isoprene, monoterpenes, and aromatic VOCs as parent hydrocarbons, which are oxidized by the hydroxyl radical (OH), O_3 , nitrate radical (NO_3) and yield three isoprene SOA, four terpene SOA, and four aromatic SOA products. For isoprene SOA, we replace the three volatility-based products with six explicit SOA products that follow the work from Marais et al. (2016). SOA formation from terpenes, benzene, toluene, and xylene is simulated using the VBS framework with four bins.

The Simple SOA scheme implements a single lumped SOA precursor, “SOAP (SOA precursor)” with a lifetime of 1 day, which irreversibly forms a single lumped SOA tracer, “SOAS (SOA simple),” and a fixed SOA yield of 100%. SOAP emissions are calculated by scaling natural and anthropogenic emissions of isoprene, monoterpenes, and CO (Chin et al., 2002; Cubison et al., 2011; Hayes et al., 2015; Hodzic & Jimenez, 2011; P. S. Kim et al., 2015; Shrivastava et al., 2017). Biogenic sources are assumed to emit SOAP and SOAS with identical mass

Table 2
Comparison of the Four SOA Schemes Used in This Study

Scheme	SOA precursors	VBS approach	SOA aging	SOA yield	Additional description	Reference
Complex	Isoprene, terpenes, benzene, toluene, xylene	Four bins ($C^* = 0.1\text{--}100$) for terpenes, benzene, toluene, xylene	Only within VBS bins	Griffin et al. (1999), Ng et al. (2007), Shilling et al. (2009), Zhang et al. (2006)	Updated isoprene chemistry and SOA formation (Marais et al., 2016)	Pye and Seinfeld. (2010)
Simple	SOAP (scaled from isoprene, terpenes, CO emissions)	N/A	N/A	100% (irreversible formation)	SOAP 100% converted to SOAS with a lifetime of 1 day	Hayes et al. (2015), Hodzic and Jimenez (2011), Shrivastava et al. (2017)
Hodzic	Isoprene, terpenes, benzene, toluene, xylene, S/IVOCs	Six bins ($C^* = 0.01\text{--}1000$) for all precursors	Only within VBS bins	Hodzic et al. (2016), Zhang et al. (2014)	Stronger production (wall-corrected yields) and faster removal (updated H^{eff} , photolysis, oxidation by O_3)	Hodzic et al. (2016)
Jo	Isoprene, terpenes, benzene, toluene, xylene, S/IVOCs	Five bins ($C^* = 0.1\text{--}1000$) for all precursors	Within VBS bins + functionalization	Farina et al. (2010)	Chemical aging (functionalization) of SOA from aromatics and S/IVOCs (decrease in volatility)	Jo et al. (2013)

yields, whereas biomass burning and fossil fuel sources only emit SOAP. The advantage of this method compared to the VBS approach is its computational efficiency and simplicity because it does not consider the dependence of SOA yields and gas-particle partitioning on factors such as temperature, NO_x levels, and pre-existing organic mass.

The Hodzic SOA scheme considers nine precursors, including isoprene, monoterpenes, aromatic VOCs, and, additionally, S/IVOCs. In addition to the traditional SOA precursors, SOA formation by unspeci-ated organic compounds, either primarily emitted or formed by POA aging, is considered by incorporating S/IVOCs in the model. As emissions of S/IVOCs are not included in traditional emission inventories, we estimate anthropogenic and biomass burning emissions of S/IVOCs by scaling 50% of POC and 20% of NMVOCs (non-methane VOCs) emissions following the work of Jathar et al. (2014). The parent hydrocarbon species are oxidized by OH, O_3 , and NO_3 . They are allocated into six bins ($C^* = 0.01, 0.1, 1, 10, 100, 1000 \mu\text{g m}^{-3}$ at 300 K) with updated wall-corrected mass yields based on a box model (SOM; Statistical Oxidation Model) study (Hodzic et al., 2016). While these updates increase SOA formation, other removal processes are included in the Hodzic scheme. First, the scheme accounts for the volatility dependence of Henry's law solubility coefficients (H^{eff}), which enhances the dry and wet deposition of SOA. Second, photolytic loss of SOA is also included as a first-order reaction. Finally, the heterogeneous reaction of O_3 with SOA is incorporated with an uptake coefficient (γ) of 10^{-5} . The updated parameters can be found in Hodzic et al. (2016).

The Jo SOA scheme considered the same parent hydrocarbons used in the Hodzic scheme and was first implemented and tested using GEOS-Chem v9-01-02 by Jo et al. (2013), and here we implemented it in GEOS-Chem v12.0.0. Precursor species undergo oxidation in the same manner as in the Hodzic scheme and yield a total of 56 products, which are allocated and partitioned using five volatility bins ($C^* = 0.1, 1, 10, 100, 1000 \mu\text{g m}^{-3}$ at 300 K). Yield parameters of S/IVOCs are based on Hodzic et al. (2016). The rest can be found in Jo et al. (2013). The prominent feature of this scheme is the chemical aging, that is, functionalization, of SOA from aromatics and S/IVOCs. These SOA products are assumed to react with OH with a rate constant of $4 \times 10^{-11} \text{ cm}^3 \text{ molecule}^{-1} \text{ s}^{-1}$, leading to a reduction of the vapor pressure and an overall increase in SOA production.

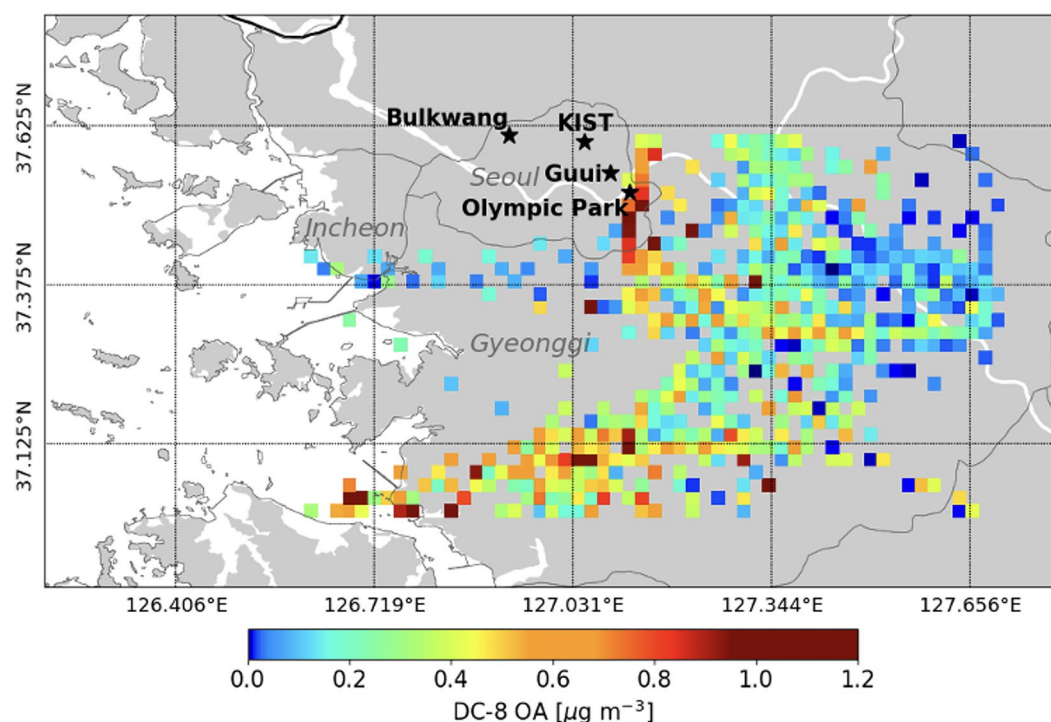


Figure 1. Map of the Seoul Metropolitan Area showing 60-s averaged OA concentrations from AMS measurements along the DC-8 flight tracks averaged below 5 km during KORUS-AQ 2016. The ground monitoring sites in Seoul used in this study are marked with black stars. Horizontal and vertical lines indicate the GEOS-Chem model grid edges with $0.25^\circ \times 0.3125^\circ$ horizontal resolution.

3. Observations

3.1. KORUS-AQ

The Korea United States Air Quality (KORUS-AQ) campaign is an international air quality field campaign that was held in Korea during spring (1 May to 10 June) 2016, which was led by the Korean National Institute of Environmental Research (NIER) and the United States National Aeronautics and Space Administration (NASA; Crawford et al., 2021). Data archived during this field campaign include aircraft and surface measurements of trace gases, aerosols, and meteorological variables, with high spatial and temporal resolutions. We use 60-s averaged airborne observations collected onboard the NASA DC-8 aircraft in the Seoul Metropolitan Area (SMA; $37\text{--}37.6^\circ\text{N}$, $126.6\text{--}128^\circ\text{E}$). We also use surface observations at several ground sites located in the northern and eastern parts of Seoul (Figure 1): Bulkwang (37.61°N , 126.93°E), KIST (Korea Institute of Science and Technology; 37.60°N , 127.05°E), Guui (37.55°N , 127.09°E), and Olympic Park (37.52°N , 127.12°E).

During the campaign, chemical compositions of non-refractory submicron particulate matter (PM_{10}) were measured using a high-resolution time-of-flight aerosol mass spectrometer (HR-ToF-AMS; Canagaratna et al., 2007; DeCarlo et al., 2006), hereafter denoted as “AMS.” Airborne (DC-8) and surface (KIST) AMS observations of OA mass concentrations were measured and further analyzed by Nault et al. (2018) and H. Kim et al. (2018), respectively, providing detailed information on the composition of OA using positive matrix factorization (PMF) analysis (Ulbrich et al., 2009). Nault et al. (2018) apportioned DC-8 observations of OA into six factors, then recombined them into three organic components: hydrocarbon-like OA (HOA), less-oxidized oxygenated OA (LO-OOA), and more-oxidized oxygenated OA (MO-OOA). We consider HOA as POA and the sum of LO-OOA and MO-OOA as SOA. H. Kim et al. (2018) applied PMF analysis to ground observations of OA at the KIST site. They identified four organic components: hydrocarbon-like OA (HOA), cooking-influenced OA (COA), low-volatility oxygenated OA (LV-OOA), and semivolatile oxygenated OA (SV-OOA). For the KIST data, we define POA as the sum of HOA and COA and SOA as the sum of LV-OOA and SV-OOA.

Table 3
Details on KORUS-AQ Observations of Gas Species Used in This Study

Species	Instrument	Institution	Reference
CO	Differential Absorption CO Measurement (DACOM)	NASA Langley Research Center	Sachse et al. (1991)
O ₃ , NO, NO ₂ , NO _y	NCAR NO _x O ₃ Chemiluminescence	National Center for Atmospheric Research	Ridley and Grahek (1990), Weinheimer et al. (1994)
VOCs	Whole Air Sampler (WAS)	University of California, Irvine	Colman et al. (2001)
Isoprene	Proton Transfer Reaction Time of Flight Mass Spectrometer (PTR-ToF-MS)	University of Innsbruck/University of Oslo	Müller et al. (2014)

Hourly ground observations of carbonaceous aerosols (OC and EC) at Bulkwang and Olympic Park were operated by NIER and the Seoul Research Institute of Public Health and Environment (SIHE), respectively. They used the semi-continuous OCEC carbon aerosol analyzer (Sunset Laboratory Inc.) based on a thermal-optical transmittance (TOT) method (Bauer et al., 2009; Birch & Cary, 1996). PMF analyses were not performed on OC observations from these sites, and therefore EC observations were used to estimate the composition of OC following the method described in Section 3.2.

Our analysis also uses supporting airborne observations of reactive gases such as CO, O₃, NO_x, NO_y (=NO_x + HNO₃ + NO₃⁻ + PAN + RONO₂), and VOCs, which are summarized in Table 3. Hourly ground observations of major gases including CO, O₃, and NO_x from the AirKorea network (<http://www.airkorea.or.kr/eng>) were provided by the Korean Ministry of Environment at the Guui and Bulkwang sites. CO, O₃, and NO_x were also measured at Olympic Park by SIHE, using real-time analyzers (Ecotech EC9830/EC9810/EC9841). Hourly timeseries of VOCs including benzene, toluene, (*o*-, *m*-, *p*-) xylenes, and isoprene at Guui and Olympic Park were measured by SIHE using gas chromatography with flame ionization detection (GC-FID, Varian Inc.). Hourly ground observations of VOCs at Bulkwang were collected using proton transfer reaction mass spectrometry (PTR-MS) by NIER.

3.2. Surface Observations

As described in the previous section, the semi-continuous OCEC analyzer measured carbonaceous aerosols. We use additional surface observations at the Bulkwang ground site for model evaluation. Supporting observations of CO, O₃, and NO₂ were provided by the AirKorea network. For model evaluation, hourly timeseries of OC and EC mass concentrations during May/July 2016, October/December 2017, and February 2018 are used. We employ the EC tracer method following Equations 1 and 2; (Turpin & Huntzicker, 1995) to estimate the primary and secondary fractions in the observed total OC, assuming that POC and EC are co-emitted from the same sources. We use Deming regression analysis to determine the primary OC to EC ratio (OC/EC)_{primary}. Refer to Section S1 in the Supporting Information S1 for a detailed description of the EC tracer method.

$$\text{POC} = (\text{OC/EC})_{\text{primary}} \times \text{EC} + (\text{OC})_{\text{non-combustion}} \quad (1)$$

$$\text{SOC} = \text{OC} - \text{POC} \quad (2)$$

Table 4 compares the Deming regression slope between ambient OC and EC, that is, (OC/EC)_{primary}, for each period and the resulting monthly mean SOA mass fractions (%), which is defined as SOA/(SOA + POA). For consistency with the model, we applied an OA/OC value of 1.3 for POC and 2.1 for SOC, as mentioned in Section 2. Note that there is a small difference (1%–7%) in total OA mass when seasonal ratios reported in observational

Table 4
(OC/EC)_{primary} Values Determined by Deming Regression Between Surface OC and EC Measurements Used in the EC Tracer Method and Resulting Monthly Mean SOA Mass Fractions (%) for Each Period

Deming fit	May 2016	July 2016	October 2017	December 2017	February 2018
(OC/EC) _{primary}	0.78 ± 0.01	1.08 ± 0.01	2.76 ± 0.10	3.20 ± 0.01	3.43 ± 0.05
SOA fraction (%)	76 ± 2	81 ± 2	41 ± 3	37 ± 2	56 ± 2

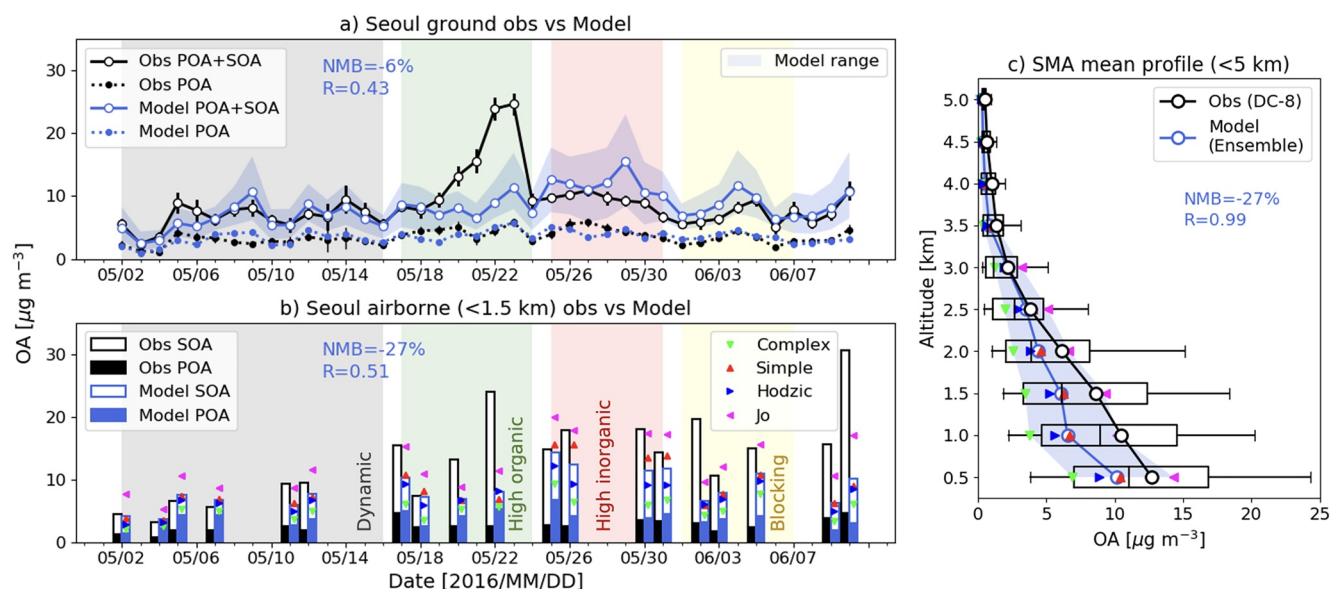


Figure 2. Comparison of observed and simulated daily mean (a) surface and (b) airborne (<1.5 km) OA, primary organic aerosols, and secondary organic aerosols concentrations at Seoul, and (c) OA vertical profiles in the Seoul Metropolitan Area (SMA) during KORUS-AQ 2016. Observations and the ensemble of all models are indicated in black and blue bars and circles, and individual models are shown in different colors and markers. In panel (a) solid lines represent daily mean OA concentrations from observations with error bars indicating the uncertainties and the ensemble model averaged at three ground sites (Bulkwang, KIST, Olympic Park) in Seoul. In panel (b) the bars indicate average values of each research flight from DC-8 observations in Seoul below 1.5 km with model values sampled coherently in time and space. Statistics (NMB, R) for the ensemble model performance are denoted above the timeseries. In panel (c) mean vertical profiles (circles) with 0.5 km intervals from DC-8 observations and model values sampled coherently along the flight tracks within the SMA are presented in different colors and markers. Boxes, whiskers, and vertical bars indicate the interquartile range, the 10th and 90th percentiles, and the median value from observations. The colored shadings indicate the synoptic periods discussed in the text.

studies (H. Kim, Zhang, et al., 2017, 2018; Huang et al., 2017; Xing et al., 2013), 1.8 (spring-summer) and 1.6 (fall-winter), are used to convert OC to OA mass.

The estimated secondary portions of the observed OA mass concentrations at the Bulkwang and Olympic Park sites during KORUS-AQ are 62% and 53%, respectively. PMF results at the KIST site for the same period showed that 61% of observed OA mass was related to secondary formation. The secondary fraction may differ on a local scale, on whether the measurement site is affected by factors such as heavy traffic, residential emissions, or biogenic emissions (Robinson et al., 2007). All three sites are located near busy roads surrounded by large residential areas. The EC tracer method shows consistent results with the PMF analysis results for surface air in Seoul regarding the various local environments surrounding each measurement site.

4. Model Evaluation During KORUS-AQ

4.1. Total OA and SOA Precursors

Figure 2 compares daily mean timeseries of observed and simulated total OA (=POA + SOA) concentrations using different SOA schemes at Seoul during 1 May–10 June 2016. Surface values were averaged at three ground sites (Bulkwang, KIST, Olympic Park) and compared to the closest model grid box values. AMS observations of POA and SOA, characterized using PMF analysis, in the boundary layer (<1.5 km) along the DC-8 flight track over Seoul (37.4–37.6°N, 127–127.2°E) are compared with simulated OA concentrations, which were sampled coherently in time and space. Mean vertical profiles within the SMA from the ground to 5 km are also shown for comparison.

Observed total OA concentrations at the ground sites and onboard the DC-8 show similar temporal variations, with a distinct peak during 19–24 May, caused by a considerable enhancement of SOA. PMF results showed that SOA observed at KIST and onboard the DC-8 during this period were more likely to be aged and less volatile, indicating that photochemistry and aging processes associated with long-range transport enhanced SOA formation (H. Kim et al., 2018; Nault et al., 2018).

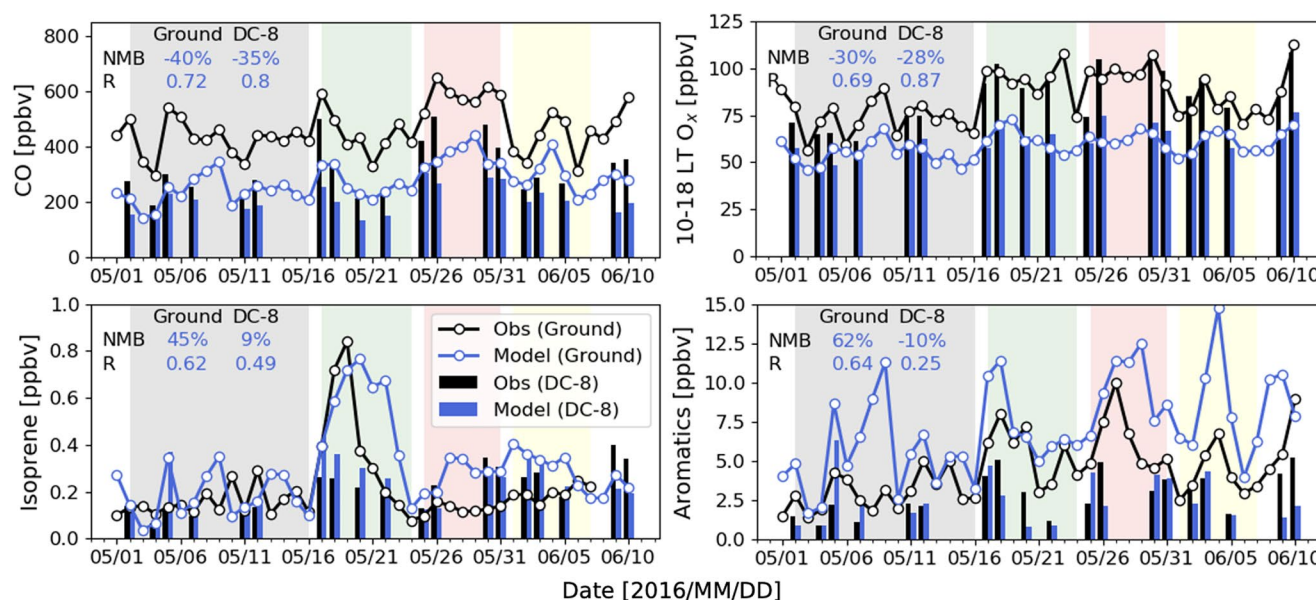


Figure 3. Comparison of observed and simulated daily mean CO, daytime (10:00–18:00 local time) O_x ($=O_3 + NO_2$), and secondary organic aerosols precursors including aromatic VOCs ($=$ benzene + toluene + xylenes) and isoprene at Seoul during KORUS-AQ 2016. Solid lines and bars indicate surface timeseries and average values of each research flight onboard the DC-8, respectively. Daily mean timeseries averaged at three ground sites (Bulkwang, Guui, Olympic Park) were used to represent the observed and simulated surface concentrations. DC-8 observations in Seoul below 1.5 km were used, and model values were sampled coherently in time and space. The model performance statistics (NMB, R) are denoted in upper-left corners. The colored shadings indicate the synoptic periods discussed in the text.

The ensemble model, representing the arithmetic mean of the four schemes, shows a 6% underestimation compared to ground observations of total OA, with normalized mean biases (NMB) from individual schemes ranging from -42% to 35% (Figure 2a). Pearson correlation coefficients (R) between the simulations and observation lie within 0.24–0.58. Overall, the Jo scheme simulates the highest OA concentrations followed by the Simple scheme, which lies between the amounts simulated by the Hodzic and Jo schemes. The Hodzic and Jo schemes better represent daily variations of observed OA ($R \geq 0.42$) compared to the Simple scheme ($R = 0.24$).

All schemes except for the Jo scheme (NMB = 8%) underestimate (NMB = -24% to -55%) airborne observations of total OA in the boundary layer, with correlation coefficients ranging from 0.37 to 0.59 (Figure 2b). The ensemble model underestimates OA in the Seoul boundary layer by 27%, with a temporal correlation coefficient of 0.51. Underestimation is consistently shown in the Complex scheme (NMB = -43% and -55% in surface air and the boundary layer, respectively), indicating that additional sources and updated yield parameters are necessary for reproducing observed OA concentrations in Seoul.

The observed vertical distribution of total OA in the SMA from the ground to 5 km is well captured by all schemes ($R \geq 0.96$) but is underestimated by the ensemble model (Figure 2c). Unlike OA, we do not find any significant model biases in simulated surface SIA (Figure S2 in Supporting Information S1) and its precursors (not shown), implying that physical processes such as aerosol deposition are less likely to be the cause of OA underestimation. Moreover, Luo et al. (2020) investigated model sensitivity to changes in wet processes using GEOS-Chem and found that updates in parameters for aqueous-phase chemistry, cloud microphysics, and wet scavenging improved SIA simulations but had minor impacts on OA simulations.

In order to investigate the cause of the model-observation discrepancies, we also compare observed and simulated SOA precursors for KORUS-AQ. Figure 3 shows the daily mean timeseries of gaseous species at the Bulkwang, Guui, and Olympic Park ground sites and in the boundary layer along the DC-8 flight track over Seoul. CO, which is used as a tracer for estimating fossil fuel and biomass burning emissions of SOAP in the Simple scheme, is consistently underestimated compared to both ground and airborne observations. This issue was addressed in several studies as an uncertainty in the KORUS v5 bottom-up emissions inventory (Gaubert et al., 2020; Park et al., 2021). Among the significant biogenic species, isoprene is overestimated at the surface (NMB = 45%) and in the boundary layer (NMB = 9%). Simulated aromatics ($=$ benzene + toluene + xylene) are also overestimated compared to ground observations but generally follow the observed daily variations. In contrast, the model shows

an underestimation and poor correlation compared to airborne observations. This discrepancy may imply model uncertainties associated with boundary layer mixing and gas-phase chemistry, requiring additional validation sensitivity tests.

Daily variations of precursor species were likely to be highly influenced by synoptic patterns (Peterson et al., 2019). In the following paragraphs, we evaluate model performance regarding the effect of meteorological conditions on SOA and its precursors. Four different synoptic periods are indicated in colored shadings in Figures 2 and 3, and the remainder of this study.

4.1.1. Dynamic Weather Period (1–16 May)

The first 2 weeks of May were characterized as a dynamic weather period with frequent precipitation and relatively strong surface wind (Figure S2 in Supporting Information S1). As a result, observed surface VOCs and daytime (10:00–18:00 local time; LT) $O_x (=O_3 + NO_2)$ levels (Figure 3) were low due to suppressed photochemical activity and strong dynamic forcing during this period. Although precipitation amounts are slightly underestimated in the model (Figure S2 in Supporting Information S1), rain events and strong winds are well represented compared to surface observations. However, simulated diurnal variations of aromatic species during this period show sharp nighttime through early morning peaks caused by too low nighttime boundary layer heights in the model (Oak et al., 2019), resulting in overestimations of daily mean values.

4.1.2. High Organic Period (17–24 May)

This period was influenced by stagnation and large-scale subsidence (Peterson et al., 2019), resulting in the weaker surface wind with warm and dry conditions (Figure S2 in Supporting Information S1). Increased anthropogenic VOCs concentrations show the effect of local emissions and accumulation under stagnant meteorology (Figure 3). Daytime O_x levels were also increased (Figure 3), implying enhanced photochemistry due to increased temperature and high precursor concentrations (H. Kim et al., 2018).

Unlike inorganic aerosol (i.e., SIA) formation, which favors humid conditions (Liu et al., 2018), observed SOA concentrations at Seoul during KORUS-AQ show a negative relationship with relative humidity (RH; Figure S3 in Supporting Information S1). Observational studies found that photochemistry was suppressed under high RH conditions, and larger anthropogenic SOA mass loadings and yields were observed with lower RH due to increased formation of oligomers in the absence of seed particles (Hinks et al., 2018; Liang et al., 2019; Liu et al., 2019; Zhang et al., 2019). Total PM loading and inorganic aerosol concentrations were particularly low during this period (Figure S2 in Supporting Information S1), providing a less-favorable condition for particle growth onto existing aerosols. This also implies that along with increased VOC oxidation via local photochemistry, enhanced oligomerization of oxidized VOCs may have contributed to SOA formation during 19–24 May.

All schemes fail to simulate SOA enhancement during the high organic period (Figure 2), although simulated precursor VOCs concentrations do not show any negative biases from observations (Figure 3). While the model simulates larger cloud fractions than observations (Figure S2 in Supporting Information S1), insufficient photochemistry or missing sources from transboundary transport may have contributed to the underestimation of SOA formation. Due to SOA underestimation, the model ensemble does not display a clear negative relationship with RH (Figure S3 in Supporting Information S1).

4.1.3. High Inorganic Period (25–31 May)

Seoul experienced extreme $PM_{2.5}$ pollution, frequently exceeding the Korean 24-hr standard of $35 \mu g m^{-3}$ (Figure S2 in Supporting Information S1), and bad visibility during 25–31 May (Jordan et al., 2020) due to a mixture of local emissions and transport of pollutants from China caused by predominant westerlies and frontal passages (Choi et al., 2019; Peterson et al., 2019). Observed SIA concentrations and anthropogenic pollutants such as CO and aromatic VOCs showed noticeable elevations (Figure S2 in Supporting Information S1, Figure 3) during this period, and POA also showed a gradual increase during 25–27 May (Figure 2). However, despite the abundance of precursor VOCs, observed SOA concentrations remained flat and relatively low compared to 17–22 May.

SOA formation is affected by the total abundance of SOA precursors and the relative contribution of precursors with high reactivities and high SOA yields, for example, toluene. We find that the observed toluene to benzene ratio was lower during this period than the high organic period, especially due to the increase of benzene, which may have caused less efficient SOA formation. In addition, as photochemistry plays a dominant role in SOA

formation during the springtime (H. Kim et al., 2018), high RH (50%–80%) seems to have suppressed SOA formation in the aqueous phase for this case (Figure S3 in Supporting Information S1).

Simulated fine PM, SIA, CO, and aromatic VOCs tend to follow the observed fluctuations, showing that the model successfully captures the eastward transport of anthropogenic pollutants. However, high precursor concentrations cause the overestimation of SOA in the Simple and Jo schemes (Figure 2), as the SOA timeseries from both schemes generally follow the timeseries characteristics of their main precursor species: CO and aromatics. Also, as a constant emission ratio (10:1) was applied to split lumped aromatic emissions into toluene and benzene in the model, the ambient ratio remains nearly unaltered, causing model-observation discrepancies in the toluene to benzene ratio.

4.1.4. Blocking Pattern Period (1–7 June)

During 1–7 June, a blocking pattern that consisted of a high-pressure system located north of a low, characterized as a “Rex Block” (Rex, 1950), caused stagnant conditions and inhibited the long-range transport of pollutants to the Korean peninsula, which resulted in accumulation of local pollutants (Jordan et al., 2020; Peterson et al., 2019). Compared to the stagnation period (17–24 May), which showed high OA levels, not only were surface conditions less stagnant (Peterson et al., 2019) but also larger cloud fractions suppressed photochemistry (Figure S2 in Supporting Information S1), causing lower SOA (Figure 2) and O_x levels (Figure 3). While surface observations showed that SOA and daytime O_x levels were 60% and 14% lower during this period than the earlier stagnation period, simulated SOA was higher by 19%, and O_x levels were lower by only 4%. The model also shows considerable overestimations of aromatic VOCs (Figure 3) and SIA (Figure S2 in Supporting Information S1) caused by peaks during 21:00–06:00 LT, mainly due to the shallow nighttime boundary layer in the model, similar to that during the dynamic weather period. Simulated diurnal profiles of aromatics and SOA during this period show similar variations, indicating that the shallow boundary layer and overestimation of precursor VOCs are likely the main cause of SOA overestimation.

4.2. Photochemical Evolution of SOA

In this section, we analyze the photochemical evolution of observed and simulated SOA during KORUS-AQ to investigate the degree of atmospheric aging and its effect on the formation and loss processes of SOA. To account for the dilution of SOA with background air during its formation, we use the dilution-corrected CO (ΔCO) and calculate photochemical age using NO_x , NO_y , and aromatic hydrocarbons.

CO is a relatively inert tracer with an atmospheric lifetime of 1 month and is primarily emitted from biomass burning and fossil fuel sources (Gaubert et al., 2020; Lee-Taylor et al., 2011). While fossil fuel use dominates CO emissions in East Asia, the ratio of ambient OA to CO enhancement, ΔCO ($=CO_{\text{ambient}} - CO_{\text{background}}$), can be used as a proxy to investigate local OA formation from anthropogenic sources and account for the effect of dilution and boundary layer dynamics (DeCarlo et al., 2010; Lee-Taylor et al., 2011; Woody et al., 2016). The estimation of enhancement ratios tends to depend highly on the $CO_{\text{background}}$ value and therefore is often defined as the slope of the regression between ambient OA and CO (de Gouw & Jimenez, 2009). In this section, we use $CO_{\text{background}}$ values based on observational analysis and a tagged CO simulation. In Section 5, we use the slope of reduced major axis (RMA) regression between ambient OA and CO to estimate the enhancement ratios.

We use a background value of 200 ppbv, which Nault et al. (2018) identified using back trajectory analysis to represent the observed $CO_{\text{background}}$ in Korea during KORUS-AQ. Because CO concentrations are underestimated in the model (Figure 3), using the same background value (200 ppbv) will cause severe underestimation of ΔCO . Therefore, to identify the simulated $CO_{\text{background}}$ value, we conducted a tagged CO simulation for the KORUS-AQ period using GEOS-Chem v12.6.3 with the identical meteorology and emissions that we used for model evaluation. In the tagged CO simulation, CO is tagged by its source region, emission type, and chemical formation process to quantify the contribution of each source to ambient CO concentrations. We define Korea's background CO as the sum of CO produced by the oxidation of hydrocarbons and from foreign anthropogenic and biomass burning sources. The resulting tagged CO simulation showed that the simulated average background CO in the boundary layer is 127 ppbv.

For photochemical age calculation, we incorporate the NO_x/NO_y clock (Kleinman et al., 2008) for the model results and the airborne observations. We investigate the photochemical processing of SOA for ages less than

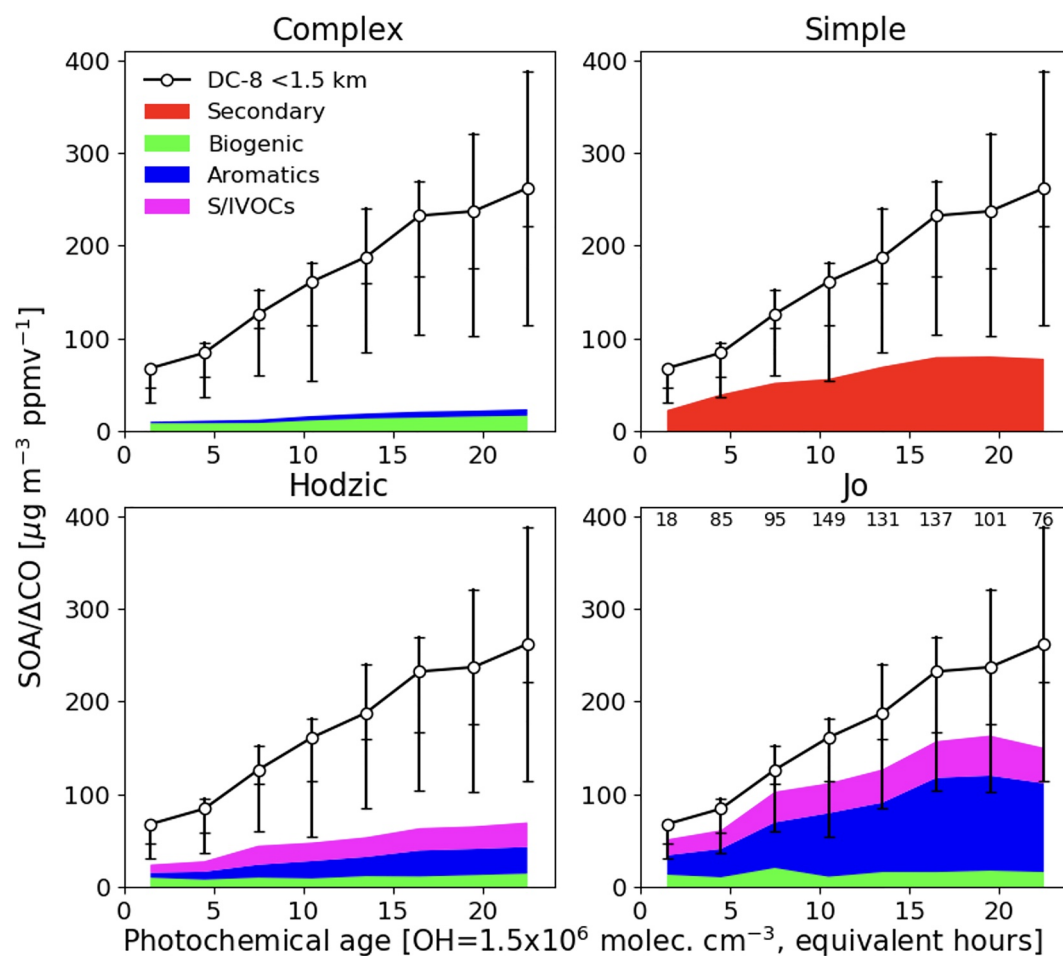


Figure 4. Observed and simulated mean secondary organic aerosols/ ΔCO ratios versus photochemical age calculated along the DC-8 flight tracks in the Seoul Metropolitan Area below 1.5 km during KORUS-AQ 2016. The number of data points used for binning is denoted in the lower-right (Jo) panel. Vertical bars indicate the interquartile range and the median of observed values.

one equivalent day due to the atmospheric nature and chemical characteristics of the NO_x/NO_y clock (Nault et al., 2018). We calculated photochemical age at the KIST ground site using the (*m*-, *p*-) xylene/ethylbenzene (X/E) clock (Parrish et al., 2007) due to lack of NO_y observations, but found that air masses in surface air were generally less aged, with an average age of 7 hours. Therefore in this section, we use airborne PMF analysis results of AMS observations in the SMA to focus on the evolution of SOA under aged conditions. Refer to Section S2 in Supporting Information S1 for a detailed description of the calculation of photochemical age.

We find that the observed POA/ ΔCO ratio remains flat with an average value of $20 \mu\text{g m}^{-3} \text{ppmv}^{-1}$, showing no distinct relationship with photochemical age. Therefore, we focus on the SOA evolution and compare observed and simulated SOA/ ΔCO ratios in the SMA boundary layer. Note that we do not account for the background value of SOA, assuming that the majority of SOA in the SMA is formed on a local scale based on observational analysis (Nault et al., 2018).

Figure 4 shows that the observed airborne SOA/ ΔCO ratio gradually increases with photochemical age, with a sharp gradient between 5–15 hr. We find that the observed tendency is also dependent on the flight altitude, where both the SOA/ ΔCO ratio (not shown) and photochemical age increase with altitude (Figure S4c in Supporting Information S1). Simulated SOA/ ΔCO ratios in the boundary layer are underestimated compared to airborne observations, regardless of SOA schemes. This is consistent with model evaluation results in Section 4, where all models underestimated the observed vertical profile of OA mass concentrations. The Jo scheme best represents the observed rapid formation between 5–8 hr among the four schemes. A noticeable increase in the

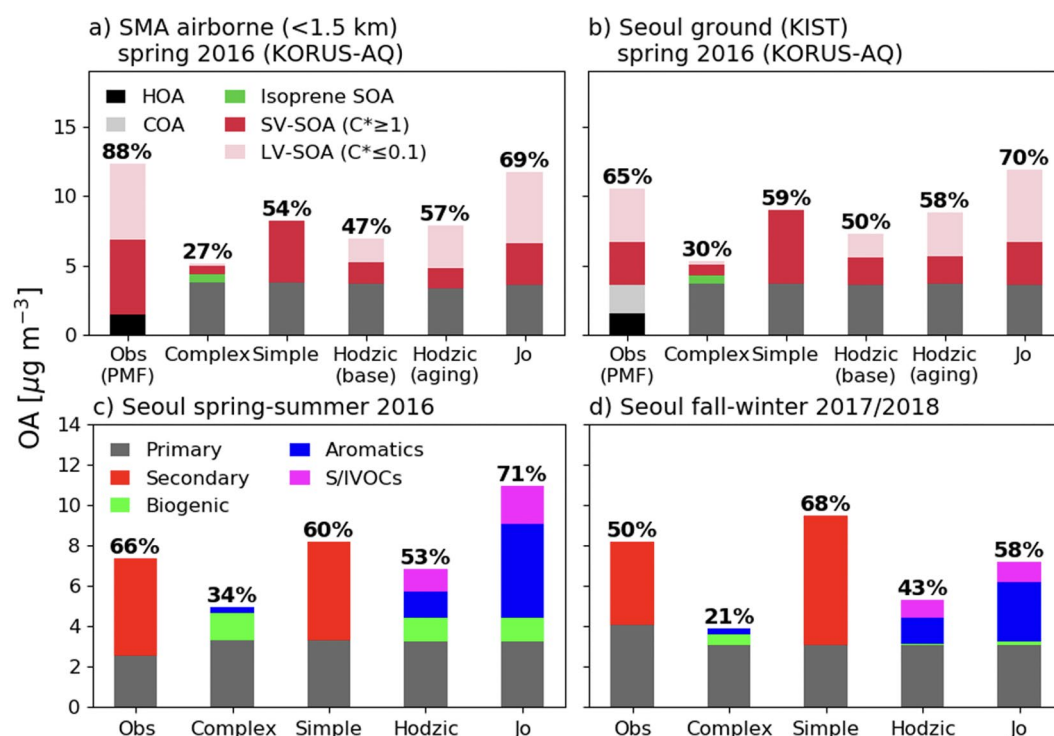


Figure 5. Comparison of observed and simulated mean OA concentrations (a–b) in the Seoul Metropolitan Area boundary layer and at the KIST ground site during KORUS-AQ and (c–d) at Seoul ground sites during different seasons. Observed and simulated secondary organic aerosols (SOA fractions) (%) are denoted above each bar. All comparisons except for (a) are based on surface data. In panels (a–b) PMF-resolved OA components during KORUS-AQ are compared with simulated results. HOA and COA represent the primary component of observed OA. Semivolatile SOA (SV-SOA) and low-volatility SOA (LV-SOA) represent the secondary component of observed OA. SV-SOA refers to SOA with $C^* \geq 1$ and the rest are defined as LV-SOA in the model. See Section 3.1 for details on PMF analyses during KORUS-AQ.

aromatic SOA portion in the Jo scheme results from the additional functionalization process. However, while observed SOA production continues to increase between 20–24 hr, simulated SOA production peaks before 20 hr and either remains flat or declines afterward, explaining the cause of SOA underestimation during 17–22 May. Overall comparison of observed and simulated enhancement ratios suggests that most schemes underpredict SOA aging in the boundary layer.

4.3. Impact of Chemical Aging on Simulated SOA

Model evaluation of our four SOA schemes shows that the inclusion of S/IVOCs and chemical aging, that is, functionalization, of SOA can improve the skill of the OA simulation. However, among the SOA schemes that incorporate S/IVOCs as SOA precursors, the Hodzic scheme often underestimates observed surface SOA concentrations. The Jo scheme tends to show overestimation due to the significant enhancement of the aromatic SOA portion. Therefore in this section, we further examine the effect of chemical aging on simulated OA by conducting a sensitivity simulation combining the two schemes. With the updates of wall-corrected SOA yields from Zhang et al. (2014), volatility-dependent H^{eff} , photolytic loss of SOA, and heterogeneous oxidation by O_3 in the model, we can attain a better representation of SOA formation and loss processes, and at the same time consider additional decreases of volatility and increases in organic mass through SOA aging via functionalization.

Figures 5a and 5b compare results of PMF analyses and model performance during the KORUS-AQ period with the inclusion of chemical aging using an aging constant of $4 \times 10^{-11} \text{ cm}^3 \text{ molecule}^{-1} \text{ s}^{-1}$ to the Hodzic scheme. Semivolatile SOA (SV-SOA) and low-volatility SOA (LV-SOA) represent the oxidized components (OOA) of observed OA. SV-SOA refers to SOA with $C^* \geq 1$ and the rest are defined as LV-SOA in the model. Chemical aging of aromatic SOA increases simulated total SOA concentrations by 14%–22% in the SMA. We find that the simulated mass of low-volatility ($C^* \leq 0.1$) SOA increases by 27%–40%, while the semivolatile ($C^* \geq 1$) portion

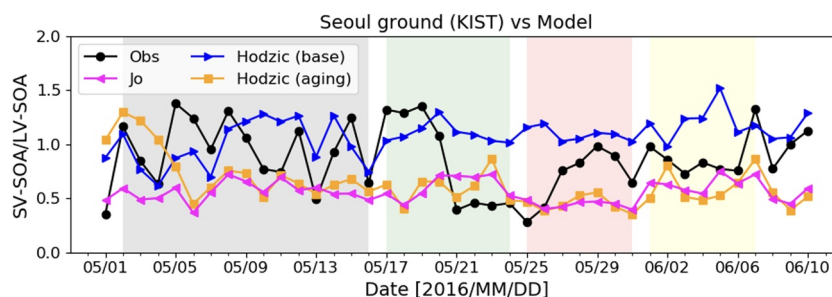


Figure 6. Comparison of observed and simulated SV-SOA/LV-SOA ratios during KORUS-AQ 2016. positive matrix factorization analyses using AMS observations at the KIST ground site in Seoul are compared with simulated results using the Hodzic, aging Hodzic, and Jo schemes. The colored shadings indicate the synoptic periods discussed in Section 4.

remains unaltered. Although all our models, including the aging Hodzic and Jo schemes, underestimate SOA formation in higher altitudes within the boundary layer, the aging Hodzic scheme shows the best performance in reproducing observed SOA in surface air.

Despite the improvement in model performance, we still find that the model fails to capture significant peaks (e.g., 16–24 May) that were noticeable in observed surface timeseries (Figure 2a). Figure 6 compares observed and simulated SV-SOA/LV-SOA ratios during KORUS-AQ 2016. Observed surface ratios during the high organic period show a sharp decrease at 21 May, indicating that observed SOA was more likely to be aged than freshly produced. As potential influences of Siberian wildfires during 16–24 May were discussed in previous studies (Kang et al., 2020; Peterson et al., 2019), chemical aging during the long-range transport of OA emitted from biomass burning sources may have resulted in the elevation of the LV-SOA portion. However, all models fail to capture this rapid change in SOA composition, regardless of the chemical aging process, indicating possible missing sources of SOA from biomass burning sources. Several studies reported that the GFED biomass burning emissions underestimate POA emissions (Lou et al., 2020) and also found that a simple empirical treatment that accounts for the aging of POA from biomass burning sources to form SOA shows good performance in simulating surface OA loadings (Lou et al., 2020). These implications call for additional sensitivity tests for the KORUS-AQ period but are beyond the scope of this paper.

5. Seasonal Characteristics of OA in Surface Air

5.1. Spring-Summer Season

In addition to the KORUS-AQ period evaluation, we evaluate simulated results during summer 2016 using surface OCEC measurements and the EC tracer method at the Bulkwang site in Seoul. Previous studies using PMF analyses to resolve OA sources in Seoul reported that ~75% of observed total OA comprised SOA during summer 2014, with the SV-OOA component being more dominant than LV-OOA (J. H. Kim, Park, et al., 2017; Park et al., 2018). J. H. Kim, Park, et al. (2017) found that among the three SOA factors that were resolved, 25% showed the characteristics of semivolatile POA, reflecting the effect of POA aging during the summer season.

Figures 5a–5c compare observed and simulated mean POA and SOA concentrations in the boundary layer in the SMA and at ground sites in Seoul during May and July 2016. We find that PMF results using airborne (DC-8) AMS measurements show a large secondary fraction (88%) and a relatively small primary fraction. Observed surface SOA during spring-summer makes up 66% of total OA mass in Seoul, resulting in a more significant primary fraction than the airborne data. PMF analysis of surface OA implies that this discrepancy may be due to the influence of cooking-related primary organic emissions, resolved as the COA factor, which is more likely to be captured in surface air (H. Kim et al., 2018). Therefore, the POA fraction in DC-8 observations can be interpreted as a lower limit in the SMA boundary layer.

Simulated POA concentrations are consistently overestimated compared to observations during the spring and summer seasons, implying either an overestimation of POA emissions or that the semivolatility of POA should be considered in models. As discussed in previous sections, the Jo and Simple schemes simulate the largest amounts of SOA, resulting in similar SOA fractions (61–71%) with surface observations, but overestimating mass

concentrations. Aromatics and S/IVOCs are the main contributors to SOA formation in the Jo scheme, indicating that considering SOA aging only through functionalization, when aging involves several other pathways in the atmosphere, including fragmentation (Chacon-Madrid & Donahue, 2011), may cause overestimation in surface air.

Noticeable portions in simulated biogenic contributions occur in warm seasons due to increased temperature and biogenic emissions (Table 1) compared to other seasons. As a result of increased biogenic emissions, observed surface isoprene concentrations during July were 3.6 times higher on average than May, whereas aromatic VOCs levels were comparable (not shown). We also find that the contribution of aromatics to simulated SOA in the Jo scheme is even larger than that during May, which can be explained by increased chemical aging due to elevated OH during the summer season.

Observed hourly OA and O_3 at Seoul during the summer are tightly correlated with a higher correlation coefficient than during the spring season (Figures S5a–S5b in Supporting Information S1). Simulated OA using the Hodzic and Jo schemes among the different SOA schemes show the highest correlations with simulated O_3 concentrations. In contrast, the photochemical relationship is not shown in the Simple scheme. Despite the increase of biogenic VOCs and the strong impact of photochemistry, observed OA mass during July is smaller than May. Simulated results from the Hodzic and Jo schemes show that SOA from aromatics and S/IVOCs have decreased compared to May, resulting in an overall decrease of total SOA mass.

5.2. Fall-Winter Season

We conducted additional simulations for the fall-winter season of 2017/2018 using the same model configurations described in Section 2. Although anthropogenic emissions from the KORUS v5 inventory are based on 2015 estimates, we did not apply additional scaling or projections as previous studies and statistics showed that anthropogenic emissions in Korea did not show significant annual trends from 2015 through 2018 (NIER, 2020). We evaluate simulated results using surface OCEC measurements and the EC tracer method at the Bulkwang site.

Park et al. (2018) performed PMF analysis of OA measurements at the Bulkwang site during fall-winter 2014 and found that the observed POA fraction was ~30%. PMF analysis of OA measurements at the KIST site during winter 2015/2016 showed that 59% of total OA mass was characterized as POA, with a significant contribution of biomass burning-related sources (H. Kim, Zhang, et al., 2017). A similar analysis by Schroder et al. (2018) also found that 42% of airborne observations of total OA during winter 2015 in the northeast US was primary, with a 33% contribution from biomass burning.

Figure 5d compares observed and simulated mean surface POA and SOA concentrations at Seoul during October, December 2017, and February 2018. Estimated POA concentrations using OC and EC observations are significantly higher than those during spring and summer, reflecting the observed seasonal variation of EC caused by increased residential or open heating and prevailing westerlies carrying pollutants from upwind regions (Park et al., 2015). However, the models tend to underestimate observed POA concentrations and show lower POA concentrations during the fall-winter period compared to the spring-summer period.

Most POA emissions in the KORUS v5 inventory are from mobile on-road transportation in Seoul. According to the Korea Expressway Cooperation (<http://www.ex.co.kr>) and Seoul Transport Operation and Information Service (<https://topis.seoul.go.kr/>), traffic volumes in Seoul and nearby expressways tend to increase with temperature and decrease with bad weather such as rain or snow, resulting in higher traffic during spring and summer than in winter. Therefore, the seasonal variation of traffic emissions is imposed in total anthropogenic POA emissions (Table 1), which results in low simulated POA concentrations during the fall-winter period. The mismatch between the seasonalities of POA emissions from KORUS v5 and observed carbonaceous aerosols calls for revision of bottom-up emissions.

Observed SOA fractions at Seoul are smaller than 50%, and OA concentrations show a relatively weak correlation with photochemistry during the fall-winter period (Figures S5c–S5e in Supporting Information S1). The Simple and Jo schemes overestimate simulated SOA concentrations and SOA fractions. Although underestimation of CO is more evident during this period (NMB = –56 to –66%) compared to spring-summer (NMB = –16 to –40%), the Simple scheme simulates excess SOA, indicating that either the SOAP emissions scaled from CO emissions are too large or the assumed lifetime (1 day) of SOAP may be too short causing the rapid formation of SOA in the

Table 5
Comparison of Observed and Simulated Seasonal $\Delta\text{OA}/\Delta\text{CO}$ Obtained From RMA Regression Between Surface OA and CO

Regression slope	Spring-summer		Fall-winter	
	Observation	Model (Ensemble)	Observation	Model (Ensemble)
$\Delta\text{OA}/\Delta\text{CO}$	38 ± 2	39 ± 1	15 ± 0	30 ± 1
$\Delta\text{POA}/\Delta\text{CO}$	6 ± 0	17 ± 0	8 ± 0	13 ± 0
$\Delta\text{SOA}/\Delta\text{CO}$	35 ± 2	27 ± 1	10 ± 0	20 ± 1

fall-winter seasons in Seoul. On the other hand, simulated aromatic VOCs are generally overestimated in the model (not shown), resulting in an overestimation of SOA simulated from the Jo scheme.

Table 5 compares observed and simulated OA to CO enhancement ratios (i.e., RMA regression slope of OA vs. CO) during different seasons. The observed $\Delta\text{OA}/\Delta\text{CO}$ value during spring-summer is $38 \mu\text{g m}^{-3} \text{ppmv}^{-1}$, 2.5 times larger than that during fall-winter. The ensemble mean of simulated surface $\Delta\text{OA}/\Delta\text{CO}$ ratios is well reproduced during spring-summer, but this is because the model biases in POA and SOA cancel each other out. During fall-winter, overestimation of both the $\Delta\text{POA}/\Delta\text{CO}$ and $\Delta\text{SOA}/\Delta\text{CO}$ ratios results in an overestimation of simulated $\Delta\text{OA}/\Delta\text{CO}$.

6. Summary and Conclusions

A 3-D global CTM, GEOS-Chem, was used to simulate OA in Seoul using four different SOA schemes (Complex, Simple, Hodzic, Jo) during spring-summer 2016 and fall-winter 2017/2018. The Complex SOA scheme uses the VBS approach and simulates SOA formed from traditional parent hydrocarbons, including isoprene, monoterpenes, and aromatic hydrocarbons. The Simple SOA scheme implements a single lumped SOA precursor, whose emissions are estimated by scaling anthropogenic and biomass burning CO and biogenic VOCs emissions, and irreversibly forms a single lumped SOA product. The Hodzic and Jo schemes both use the VBS approach and simulate SOA formed from isoprene, monoterpenes, aromatics, and additionally S/IVOCs. The Hodzic scheme uses updated SOA yields, H^{eff} , and additional SOA removal pathways, boosting both the sources and sinks of SOA. The Jo scheme considers the chemical aging of aromatic SOA, which increases SOA mass.

For model evaluation, we used ground and airborne OA (OC) observations measured using the AMS and OCEC carbon analyzer. We found that simulated POA was overestimated during spring-summer but underestimated during fall-winter. During the spring-summer seasons, the Jo scheme simulated the highest SOA concentrations, followed by the Simple and Hodzic schemes. The Complex scheme underestimated observed SOA concentrations compared to the Hodzic and Jo schemes, regardless of seasons. The Simple scheme simulated the largest amounts during fall-winter, followed by the Jo and Hodzic schemes. Overall, model evaluation for SOA at Seoul showed that:

1. The Complex scheme severely underestimated observed SOA concentrations, emphasizing the critical role of S/IVOCs as SOA precursors.
2. The Simple scheme generally overestimated observed SOA concentrations, implying uncertainties in the representation of SOAP emissions and the lifetime of SOAP.
3. The Hodzic scheme slightly underestimated observed SOA concentrations but reproduced observed photochemical characteristics of SOA.
4. The Jo scheme generally overestimated observed SOA concentrations with significant enhancements of the aromatic contribution due to chemical aging.
5. The inclusion of chemical aging to the Hodzic scheme resulted in a 14%–22% increase of simulated SOA during May 2016 due to the increase of low-volatility SOA.

To conclude, for better model representation of SOA formation in urban environments such as in Seoul, we recommend the inclusion of additional S/IVOCs precursors and chemical aging processes of SOA. For computational efficiency, the Simple SOA scheme is a good alternative but can lead to biases associated with bottom-up CO emissions depending on the study region.

Data Availability Statement

Ground observations of $\text{PM}_{2.5}$, CO, O_3 , and NO_2 in Korea are available online through <https://www.airkorea.or.kr/web> (in Korean). Data from KORUS-AQ are available online through <https://doi.org/10.5067/Suborbital/KORUSAQ/DATA01>. GEOS-Chem simulation results are available upon request.

Acknowledgments

We thank all members of the KORUS-AQ, NIER, SIHE instrument teams for providing measurements onboard the DC-8 and ground sites in Seoul. This work was supported by the National Research Foundation of Korea (NRF) grant funded by the Korean Ministry of Science and ICT (MSIT; NRF-2018R1A2B3004494, NRF-2018R1A5A1024958), and the NIER, funded by the Ministry of Environment (ME) of the Republic of Korea (NIER-2020-04-02-086 and NIER-2021-04-02-189). B. A. Nault, P. C. Jost, and J. L. Jimenez, acknowledge the support by NASA grants NNX15AT96G, 80NSSC19K0124, and 80NSSC18K0630. PTR-ToF-MS measurements aboard the NASA DC-8 during KORUS-AQ were supported by the Austrian Federal Ministry for Transport, Innovation and Technology (bmvit-FFG-ASAP). The PTR-MS instrument team (P. Eichler, L. Kaser, T. Mikoviny, M. Müller) is acknowledged for their support with field work and data processing.

References

- Bauer, J. J., Yu, X.-Y., Cary, R., Laulainen, N., & Berkowitz, C. (2009). Characterization of the sunset semi-continuous carbon aerosol analyzer. *Journal of the Air & Waste Management Association*, 59(7), 826–833. <https://doi.org/10.3155/1047-3289.59.7.826>
- Bey, I., Jacob Daniel, J., Yantosca Robert, M., Logan Jennifer, A., Field Brendan, D., Fiore Arlene, M., et al. (2001). Global modeling of tropospheric chemistry with assimilated meteorology: Model description and evaluation. *Journal of Geophysical Research: Atmospheres*, 106(D19), 23073–23095. <https://doi.org/10.1029/2001jd000807>
- Birch, M., & Cary, R. (1996). Elemental carbon-based method for monitoring occupational exposures to particulate diesel exhaust. *Aerosol Science and Technology*, 25, 221–241. <https://doi.org/10.1080/02786829608965393>
- Bond, T. C., Streets, D. G., Yarber, K. F., Nelson, S. M., Woo, J.-H., & Klimont, Z. (2004). A technology-based global inventory of black and organic carbon emissions from combustion. *Journal of Geophysical Research: Atmospheres*, 109(D14), D14203. <https://doi.org/10.1029/2003jd003697>
- Canagaratna, M. R., Jayne, J. T., Jimenez, J. L., Allan, J. D., Alfarra, M. R., Zhang, Q., & Worsnop, D. R. (2007). Chemical and microphysical characterization of ambient aerosols with the aerodyne aerosol mass spectrometer. *Mass Spectrometry Reviews*, 26(2), 185–222. <https://doi.org/10.1002/mas.20115>
- Chacon-Madrid, H. J., & Donahue, N. M. (2011). Fragmentation vs. functionalization: Chemical aging and organic aerosol formation. *Atmospheric Chemistry and Physics*, 11(20), 10553–10563. <https://doi.org/10.5194/acp-11-10553-2011>
- Chin, M., Ginoux, P., Kinne, S., Torres, O., Holben, B. N., Duncan, B. N., & Nakajima, T. (2002). Tropospheric aerosol optical thickness from the GOCART model and comparisons with satellite and sun photometer measurements. *Journal of the Atmospheric Sciences*, 59(3), 461–483. [https://doi.org/10.1175/1520-0469\(2002\)059<0461:TAOTFT>2.0.CO;2](https://doi.org/10.1175/1520-0469(2002)059<0461:TAOTFT>2.0.CO;2)
- Choi, J., Park, R. J., Lee, H.-M., Lee, S., Jo, D. S., Jeong, J. I., et al. (2019). Impacts of local vs. trans-boundary emissions from different sectors on PM_{2.5} exposure in South Korea during the KORUS-AQ campaign. *Atmospheric Environment*, 203, 196–205. <https://doi.org/10.1016/j.atmosenv.2019.02.008>
- Colman, J. J., Swanson, A. L., Meinardi, S., Sive, B. C., Blake, D. R., & Rowland, F. S. (2001). Description of the analysis of a wide range of volatile organic compounds in whole air samples collected during PEM-tropics A and B. *Analytical Chemistry*, 73(15), 3723–3731. <https://doi.org/10.1021/ac010027g>
- Cooke, W., Lioussse, C., Cachier, H., & Feichter, J. (1999). Construction of a 1° × 1° fossil fuel emission data set for carbonaceous aerosol and implementation and radiative impact in the ECHAM4 model. *Journal of Geophysical Research: Atmospheres*, 104(D18), 22137–22162. <https://doi.org/10.1029/1999jd900187>
- Crawford, J. H., Ahn, J.-Y., Al-Saadi, J., Chang, L., Emmons, L. K., Kim, J., et al. (2021). The Korea-United States Air Quality (KORUS-AQ) field study. *Elementa: Science of the Anthropocene*, 9(1), 1–27.
- Cubison, M. J., Ortega, A. M., Hayes, P. L., Farmer, D. K., Day, D., Lechner, M. J., et al. (2011). Effects of aging on organic aerosol from open biomass burning smoke in aircraft and laboratory studies. *Atmospheric Chemistry and Physics*, 11(23), 12049–12064. <https://doi.org/10.5194/acp-11-12049-2011>
- DeCarlo, P. F., Kimmel, J. R., Trimborn, A., Northway, M. J., Jayne, J. T., Aiken, A. C., et al. (2006). Field-deployable, high-resolution, time-of-flight aerosol mass spectrometer. *Analytical Chemistry*, 78(24), 8281–8289. <https://doi.org/10.1021/ac061249n>
- DeCarlo, P. F., Ulbrich, I. M., Crounse, J., de Foy, B., Dunlea, E. J., Aiken, A. C., et al. (2010). Investigation of the sources and processing of organic aerosol over the Central Mexican Plateau from aircraft measurements during MILAGRO. *Atmospheric Chemistry and Physics*, 10(12), 5257–5280. <https://doi.org/10.5194/acp-10-5257-2010>
- de Gouw, J., & Jimenez, J. L. (2009). Organic aerosols in the earth's atmosphere. *Environmental Science & Technology*, 43(20), 7614–7618. <https://doi.org/10.1021/es9006004>
- Donahue, N. M., Robinson, A. L., Stanier, C. O., & Pandis, S. N. (2006). Coupled partitioning, dilution, and chemical aging of semivolatile organics. *Environmental Science & Technology*, 40(8), 2635–2643. <https://doi.org/10.1021/es052297c>
- Farina, S. C., Adams, P. J., & Pandis, S. N. (2010). Modeling global secondary organic aerosol formation and processing with the volatility basis set: Implications for anthropogenic secondary organic aerosol. *Journal of Geophysical Research*, 115(D9). <https://doi.org/10.1029/2009jd013046>
- Fountoukis, C., & Nenes, A. (2007). ISORROPIA II: a computationally efficient thermodynamic equilibrium model for K⁺-Ca₂⁺-Mg₂⁺-NH₄⁺-Na⁺-SO₄²⁻-NO₃⁻-Cl⁻-H₂O aerosols. *Atmospheric Chemistry and Physics*, 7(17), 4639–4659. <https://doi.org/10.5194/acp-7-4639-2007>
- Gaubert, B., Emmons, L. K., Raeder, K., Tilmes, S., Miyazaki, K., Arellano, Jr, et al. (2020). Correcting model biases of CO in East Asia: Impact on oxidant distributions during KORUS-AQ. *Atmospheric Chemistry and Physics Discussions*, 2020, 1–49. <https://doi.org/10.5194/acp-2020-599>
- Griffin, R. J., Cocker, D. R., III, Flagan, R. C., & Seinfeld, J. H. (1999). Organic aerosol formation from the oxidation of biogenic hydrocarbons. *Journal of Geophysical Research: Atmospheres*, 104(D3), 3555–3567. <https://doi.org/10.1029/1998JD100049>
- Guenther, A. B., Jiang, X., Heald, C. L., Sakulyanontvittaya, T., Duhl, T., Emmons, L. K., & Wang, X. (2012). The model of emissions of gases and aerosols from nature version 2.1 (MEGAN2.1): An extended and updated framework for modeling biogenic emissions. *Geoscientific Model Development*, 5(6), 1471–1492. <https://doi.org/10.5194/gmd-5-1471-2012>
- Hallquist, M., Wenger, J. C., Baltensperger, U., Rudich, Y., Simpson, D., Claeys, M., et al. (2009). The formation, properties and impact of secondary organic aerosol: Current and emerging issues. *Atmospheric Chemistry and Physics*, 9(14), 5155–5236. <https://doi.org/10.5194/acp-9-5155-2009>
- Hayes, P. L., Carlton, A. G., Baker, K. R., Ahmadov, R., Washenfelder, R. A., Alvarez, S., et al. (2015). Modeling the formation and aging of secondary organic aerosols in Los Angeles during CalNex 2010. *Atmospheric Chemistry and Physics*, 15(10), 5773–5801. <https://doi.org/10.5194/acp-15-5773-2015>
- Hinks, M. L., Montoya-Aguilera, J., Ellison, L., Lin, P., Laskin, A., Laskin, J., et al. (2018). Effect of relative humidity on the composition of secondary organic aerosol from the oxidation of toluene. *Atmospheric Chemistry and Physics*, 18(3), 1643–1652. <https://doi.org/10.5194/acp-18-1643-2018>
- Hodzic, A., & Jimenez, J. L. (2011). Modeling anthropogenically controlled secondary organic aerosols in a megacity: A simplified framework for global and climate models. *Geoscientific Model Development*, 4(4), 901–917. <https://doi.org/10.5194/gmd-4-901-2011>
- Hodzic, A., Jimenez, J. L., Madronich, S., Canagaratna, M. R., DeCarlo, P. F., Kleinman, L., & Fast, J. (2010). Modeling organic aerosols in a megacity: Potential contribution of semi-volatile and intermediate volatility primary organic compounds to secondary organic aerosol formation. *Atmospheric Chemistry and Physics*, 10(12), 5491–5514. <https://doi.org/10.5194/acp-10-5491-2010>
- Hodzic, A., Kasibhatla, P. S., Jo, D. S., Cappa, C. D., Jimenez, J. L., Madronich, S., & Park, R. J. (2016). Rethinking the global secondary organic aerosol (SOA) budget: Stronger production, faster removal, shorter lifetime. *Atmospheric Chemistry and Physics*, 16(12), 7917–7941. <https://doi.org/10.5194/acp-16-7917-2016>

- Huang, X., Liu, Z., Liu, J., Hu, B., Wen, T., Tang, G., et al. (2017). Chemical characterization and source identification of PM_{2.5} at multiple sites in the Beijing–Tianjin–Hebei region, China. *Atmospheric Chemistry and Physics*, 17(21), 12941–12962. <https://doi.org/10.5194/acp-17-12941-2017>
- Jang, Y., Lee, Y., Kim, J., Kim, Y., & Woo, J.-H. (2019). Improvement China point source for improving bottom-up emission inventory. *Asia-Pacific Journal of Atmospheric Sciences*, 56(1), 107–118. <https://doi.org/10.1007/s13143-019-00115-y>
- Jathar, S. H., Gordon, T. D., Hennigan, C. J., Pye, H. O., Pouliot, G., Adams, P. J., et al. (2014). Unspeciated organic emissions from combustion sources and their influence on the secondary organic aerosol budget in the United States. *Proceedings of the National Academy of Sciences of the United States of America*, 111(29), 10473–10478. <https://doi.org/10.1073/pnas.1323740111>
- Jimenez, J. L., Canagaratna, M. R., Donahue, N. M., Prevot, A. S. H., Zhang, Q., Kroll, J. H., et al. (2009). Evolution of organic aerosols in the atmosphere. *Science*, 326(5959), 1525–1529. <https://doi.org/10.1126/science.1180353>
- Jo, D. S., Park, R. J., Kim, M. J., & Spracklen, D. V. (2013). Effects of chemical aging on global secondary organic aerosol using the volatility basis set approach. *Atmospheric Environment*, 81, 230–244. <https://doi.org/10.1016/j.atmosenv.2013.08.055>
- Jordan, C., Crawford, J., Beyersdorf, A., Eck, T., Halliday, H., Nault, B., & Schwarz, J. (2020). Investigation of factors controlling PM_{2.5} variability across the South Korean Peninsula during KORUS-AQ. *Elementa: Science of the Anthropocene*, 8, 28. <https://doi.org/10.1525/elementa.424>
- Kang, S., Park, G., Park, T., Ban, J., Kim, K., Seo, Y., et al. (2020). Semi-continuous Measurements of Water-soluble Organic Carbon and Ionic Composition of PM_{2.5} in Baengnyeong Island during the 2016 KORUS-AQ (Korea-United States Air Quality Study). *Asian Journal of Atmospheric Environment*, 14(3), 307–318. <https://doi.org/10.5572/ajae.2020.14.3.307>
- Kim, H., Zhang, Q., Bae, G. N., Kim, J. Y., & Lee, S. B. (2017). Sources and atmospheric processing of winter aerosols in Seoul, Korea: Insights from real-time measurements using a high-resolution aerosol mass spectrometer. *Atmospheric Chemistry and Physics*, 17(3), 2009–2033. <https://doi.org/10.5194/acp-17-2009-2017>
- Kim, H., Zhang, Q., & Heo, J. (2018). Influence of intense secondary aerosol formation and long-range transport on aerosol chemistry and properties in the Seoul Metropolitan area during spring time: Results from KORUS-AQ. *Atmospheric Chemistry and Physics*, 18(10), 7149–7168. <https://doi.org/10.5194/acp-18-7149-2018>
- Kim, J.-H., Park, J.-S., Choi, J.-S., Park, J.-S., Park, S.-M., Song, I.-H., et al. (2017). A study on the characteristics of PM_{1.0} and source of organic components during summertime at Seoul and Baengnyeong Island. *Journal of Korean Society for Atmospheric Environment*, 17(3), 213–230.
- Kim, P. S., Jacob, D. J., Fisher, J. A., Travis, K., Yu, K., Zhu, L., et al. (2015). Sources, seasonality, and trends of southeast US aerosol: An integrated analysis of surface, aircraft, and satellite observations with the GEOS-Chem chemical transport model. *Atmospheric Chemistry and Physics*, 15(18), 10411–10433. <https://doi.org/10.5194/acp-15-10411-2015>
- Kleinman, L. I., Springston, S. R., Daum, P. H., Lee, Y. N., Nunnermacker, L. J., Senum, G. I., & Jayne, J. (2008). The time evolution of aerosol composition over the Mexico City plateau. *Atmospheric Chemistry and Physics*, 8(6), 1559–1575. <https://doi.org/10.5194/acp-8-1559-2008>
- Landrigan, P., Fuller, R., Acosta, N., Adeyi, O., Arnold, R., Basu, N., & Zhong, M. (2017). The Lancet commission on pollution and health. *The Lancet*, 391. [https://doi.org/10.1016/S0140-6736\(17\)32345-0](https://doi.org/10.1016/S0140-6736(17)32345-0)
- Lee-Taylor, J., Madronich, S., Aumont, B., Baker, A., Camredon, M., Hodzic, A., et al. (2011). Explicit modeling of organic chemistry and secondary organic aerosol partitioning for Mexico City and its outflow plume. *Atmospheric Chemistry and Physics*, 11(24), 13219–13241. <https://doi.org/10.5194/acp-11-13219-2011>
- Liang, L., Engling, G., Cheng, Y., Zhang, X., Sun, J., Xu, W., & Ma, Q. (2019). Influence of high relative humidity on secondary organic carbon: Observations at a background site in East China. *Journal of Meteorological Research*, 33(5), 905–913. <https://doi.org/10.1007/s13351-019-8202-2>
- Liu, Q., Jia, X., Quan, J., Li, J., Li, X., Wu, Y., & Liu, Y. (2018). New positive feedback mechanism between boundary layer meteorology and secondary aerosol formation during severe haze events. *Scientific Reports*, 8(1), 6095. <https://doi.org/10.1038/s41598-018-24366-3>
- Liu, S., Tsona, N. T., Zhang, Q., Jia, L., Xu, Y., & Du, L. (2019). Influence of relative humidity on cyclohexene SOA formation from OH photooxidation. *Chemosphere*, 231, 478–486. <https://doi.org/10.1016/j.chemosphere.2019.05.131>
- Lou, S., Shrivastava, M., Easter, R., Yang, Y., Ma, P.-L., Wang, H., & Schulz, C. (2020). New SOA treatments within the energy exascale Earth system model (E3SM): Strong production and sinks govern atmospheric SOA distributions and radiative forcing. *Journal of Advances in Modeling Earth Systems*, 12. <https://doi.org/10.1029/2020MS002266>
- Luo, G., Yu, F., & Moch, J. M. (2020). Further improvement of wet process treatments in GEOS-Chem v12.6.0: Impact on global distributions of aerosols and aerosol precursors. *Geoscientific Model Development*, 13(6), 2879–2903. <https://doi.org/10.5194/gmd-13-2879-2020>
- Marais, E. A., Jacob, D. J., Jimenez, J. L., Campuzano-Jost, P., Day, D. A., Hu, W., et al. (2016). Aqueous-phase mechanism for secondary organic aerosol formation from isoprene: Application to the southeast United States and co-benefit of SO₂ emission controls. *Atmospheric Chemistry and Physics*, 16(3), 1603–1618. <https://doi.org/10.5194/acp-16-1603-2016>
- Mukherjee, A., & Agrawal, M. (2017). World air particulate matter: Sources, distribution and health effects. *Environmental Chemistry Letters*, 15(2), 283–309. <https://doi.org/10.1007/s10311-017-0611-9>
- Müller, M., Mikoviny, T., Feil, S., Haidacher, S., Hanel, G., Hartungen, E., & Wisthaler, A. (2014). A compact PTR-ToF-MS instrument for airborne measurements of volatile organic compounds at high spatiotemporal resolution. *Atmospheric Measurement Techniques*, 7(11), 3763–3772. <https://doi.org/10.5194/amt-7-3763-2014>
- Myhre, G., Shindell, D., Bréon, F.-M., Collins, W., Fuglestad, J., Huang, J., Koch, D., et al. (2013). Anthropogenic and natural radiative forcing. In T. F. Stocker, D. Qin, G.-K. Plattner, M. Tignor, S. K. Allen, J. Boschung, et al. (Eds.), *Climate change 2013: The physical science basis* (pp. 659–740).
- Nault, B. A., Campuzano-Jost, P., Day, D. A., Schroder, J. C., Anderson, B., Beyersdorf, A. J., et al. (2018). Secondary organic aerosol production from local emissions dominates the organic aerosol budget over Seoul, South Korea, during KORUS-AQ. *Atmospheric Chemistry and Physics*, 18(24), 17769–17800. <https://doi.org/10.5194/acp-18-17769-2018>
- Ng, N. L., Kroll, J. H., Chan, A. W. H., Chhabra, P. S., Flagan, R. C., & Seinfeld, J. H. (2007). Secondary organic aerosol formation from *m*-xylene, toluene, and benzene. *Atmospheric Chemistry and Physics*, 7(14), 3909–3922. <https://doi.org/10.5194/acp-7-3909-2007>
- NIER. (2020). 2017 national air pollutants emission. Retrieved from <https://Airemiss.Nier.Go.Kr/>
- NIER, & NASA. (2017). KORUS-AQ rapid science synthesis report. Retrieved from <https://espo.nasa.gov/Sites/Default/Files/Documents/KO-RUS-AQ%20RSSR.Pdf>
- Oak, Y. J., Park, R. J., Schroeder, J. R., Crawford, J. H., Blake, D. R., Weinheimer, A. J., et al. (2019). Evaluation of simulated O₃ production efficiency during the KORUS-AQ campaign: Implications for anthropogenic NO_x emissions in Korea. *Elementa: Science of the Anthropocene*, 7. <https://doi.org/10.1525/elementa.394>
- Odum, J. R., Hoffmann, T., Bowman, F., Collins, D., Flagan, R. C., & Seinfeld, J. H. (1996). Gas/particle partitioning and secondary organic aerosol yields. *Environmental Science & Technology*, 30(8), 2580–2585. <https://doi.org/10.1021/es950943>

- Pai, S. J., Heald, C. L., Pierce, J. R., Farina, S. C., Marais, E. A., Jimenez, J. L., & Vu, K. (2020). An evaluation of global organic aerosol schemes using airborne observations. *Atmospheric Chemistry and Physics*, 20(5), 2637–2665. <https://doi.org/10.5194/acp-20-2637-2020>
- Park, J. S., Song, I. H., Park, S.-M., Shin, H., & Hong, Y. (2015). The characteristics and seasonal variations of OC and EC for PM_{2.5} in Seoul Metropolitan area in 2014. *Journal of Environmental Impact Assessment*, 24(6), 578–592. <https://doi.org/10.14249/eia.2015.24.6.578>
- Park, J.-M., Han, Y.-J., Cho, S.-H., & Kim, H.-W. (2018). Characteristics of carbonaceous PM_{2.5} in a small residential city in Korea. *Atmosphere*, 9(12), 490. <https://doi.org/10.3390/atmos9120490>
- Park, R. J., Jacob, D. J., Chin, M., & Martin, R. V. (2003). Sources of carbonaceous aerosols over the United States and implications for natural visibility. *Journal of Geophysical Research: Atmospheres*, 108(D12), 4355. <https://doi.org/10.1029/2002jd003190>
- Park, R. J., Oak, Y. J., Emmons, L. K., Kim, C.-H., Pfister, G. G., Carmichael, G. R., et al. (2021). Multi-model intercomparisons of air quality simulations for the KORUS-AQ campaign. *Elementa: Science of the Anthropocene*, 9(1). <https://doi.org/10.1525/elementa.2021.00139>
- Parrish, D. D., Stohl, A., Forster, C., Atlas, E. L., Blake, D. R., Goldan, P. D., et al. (2007). Effects of mixing on evolution of hydrocarbon ratios in the troposphere. *Journal of Geophysical Research: Atmospheres*, 112(D10), D10S34. <https://doi.org/10.1029/2006JD007583>
- Peterson, D. A., Hyer, E. J., Han, S.-O., Crawford, J. H., Park, R. J., Holz, R., et al. (2019). Meteorology influencing springtime air quality, pollution transport, and visibility in Korea. *Elementa: Science of the Anthropocene*, 7. <https://doi.org/10.1525/elementa.395>
- Philip, S., Martin, R. V., Pierce, J. R., Jimenez, J. L., Zhang, Q., Canagaratna, M. R., et al. (2014). Spatially and seasonally resolved estimate of the ratio of organic mass to organic carbon. *Atmospheric Environment*, 87, 34–40. <https://doi.org/10.1016/j.atmosenv.2013.11.065>
- Pye, H. O. T., & Seinfeld, J. H. (2010). A global perspective on aerosol from low-volatility organic compounds. *Atmospheric Chemistry and Physics*, 10(9), 4377–4401. <https://doi.org/10.5194/acp-10-4377-2010>
- Rex, D. F. (1950). Blocking action in the Middle troposphere and its effect upon regional climate. *Tellus*, 2(3), 196–211. <https://doi.org/10.1111/j.2153-3490.1950.tb00331.x>
- Ridley, B. A., & Grahek, F. E. (1990). A small, low flow, high sensitivity reaction vessel for NO chemiluminescence detectors. *Journal of Atmospheric and Oceanic Technology*, 7(2), 307–311. [https://doi.org/10.1175/1520-0426\(1990\)007<0307:ASLFHS>2.0.CO;2](https://doi.org/10.1175/1520-0426(1990)007<0307:ASLFHS>2.0.CO;2)
- Robinson, A. L., Donahue, N. M., Shrivastava, M. K., Weitkamp, E. A., Sage, A. M., Grieshop, A. P., et al. (2007). Rethinking organic aerosols: Semivolatile emissions and photochemical aging. *Science*, 315(5816), 1259–1262. <https://doi.org/10.1126/science.1133061>
- Sachse, G. W., Collins, J. E., Jr, Hill, G. F., Wade, L. O., Burney, L. G., & Ritter, J. A. (1991). Airborne tunable diode laser sensor for high-precision concentration and flux measurements of carbon monoxide and methane. *Proceedings of SPIE*, 1433. <https://doi.org/10.1117/12.46162>
- Schroder, J. C., Campuzano-Jost, P., Day, D. A., Shah, V., Larson, K., Sommers, J. M., et al. (2018). Sources and secondary production of organic aerosols in the northeastern United States during WINTER. *Journal of Geophysical Research: Atmospheres*, 123(14), 7771–7796. <https://doi.org/10.1029/2018jd028475>
- Shilling, J. E., Chen, Q., King, S. M., Rosenoern, T., Kroll, J. H., Worsnop, D. R., et al. (2009). Loading-dependent elemental composition of α -pinene SOA particles. *Atmospheric Chemistry and Physics*, 9(3), 771–782. <https://doi.org/10.5194/acp-9-771-2009>
- Shrivastava, M., Cappa, C. D., Fan, J., Goldstein, A. H., Guenther, A. B., Jimenez, J. L., & Zhang, Q. (2017). Recent advances in understanding secondary organic aerosol: Implications for global climate forcing. *Reviews of Geophysics*, 55(2), 509–559. <https://doi.org/10.1002/2016RG000540>
- Shrivastava, M. K., Lane, T. E., Donahue, N. M., Pandis, S. N., & Robinson, A. L. (2008). Effects of gas particle partitioning and aging of primary emissions on urban and regional organic aerosol concentrations. *Journal of Geophysical Research*, 113(D18). <https://doi.org/10.1029/2007jd009735>
- Stanier, C. O., Donahue, N., & Pandis, S. N. (2008). Parameterization of secondary organic aerosol mass fractions from smog chamber data. *Atmospheric Environment*, 42(10), 2276–2299. <https://doi.org/10.1016/j.atmosenv.2007.12.042>
- Tsigaridis, K., Daskalakis, N., Kanakidou, M., Adams, P. J., Artaxo, P., Bahadur, R., et al. (2014). The AeroCom evaluation and intercomparison of organic aerosol in global models. *Atmospheric Chemistry and Physics*, 14(19), 10845–10895. <https://doi.org/10.5194/acp-14-10845-2014>
- Turpin, B. J., & Huntzicker, J. J. (1995). Identification of secondary organic aerosol episodes and quantitation of primary and secondary organic aerosol concentrations during SCAQS. *Atmospheric Environment*, 29(23), 3527–3544. [https://doi.org/10.1016/1352-2310\(94\)00276-Q](https://doi.org/10.1016/1352-2310(94)00276-Q)
- Ulbrich, I. M., Canagaratna, M. R., Zhang, Q., Worsnop, D. R., & Jimenez, J. L. (2009). Interpretation of organic components from Positive Matrix Factorization of aerosol mass spectrometric data. *Atmospheric Chemistry and Physics*, 9(9), 2891–2918. <https://doi.org/10.5194/acp-9-2891-2009>
- van der Werf, G. R., Randerson, J. T., Giglio, L., Collatz, G. J., Mu, M., Kasibhatla, P. S., et al. (2010). Global fire emissions and the contribution of deforestation, savanna, forest, agricultural, and peat fires (1997–2009). *Atmospheric Chemistry and Physics*, 10(23), 11707–11735. <https://doi.org/10.5194/acp-10-11707-2010>
- Wang, Q., Jacob, D. J., Spackman, J. R., Perring, A. E., Schwarz, J. P., Moteki, N., et al. (2014). Global budget and radiative forcing of black carbon aerosol: Constraints from pole-to-pole (HIPPO) observations across the Pacific. *Journal of Geophysical Research: Atmospheres*, 119(1), 195–206. <https://doi.org/10.1002/2013JD020824>
- Weinheimer, A. J., Walega, J. G., Ridley, B. A., Gary, B. L., Blake, D. R., Blake, N. J., et al. (1994). Meridional distributions of NO_x, NO_y, and other species in the lower stratosphere and upper troposphere during AASE II. *Geophysical Research Letters*, 21(23), 2583–2586. <https://doi.org/10.1029/94gl01897>
- Woo, J.-H., Choi, K.-C., Kim, H. K., Baek, B. H., Jang, M., Eum, J.-H., et al. (2012). Development of an anthropogenic emissions processing system for Asia using SMOKE. *Atmospheric Environment*, 58, 5–13. <https://doi.org/10.1016/j.atmosenv.2011.10.042>
- Woody, M. C., Baker, K. R., Hayes, P. L., Jimenez, J. L., Koo, B., & Pye, H. O. T. (2016). Understanding sources of organic aerosol during CalNex-2010 using the CMAQ-VBS. *Atmospheric Chemistry and Physics*, 16(6), 4081–4100. <https://doi.org/10.5194/acp-16-4081-2016>
- Xing, L., Fu, T. M., Cao, J. J., Lee, S. C., Wang, G. H., Ho, K. F., et al. (2013). Seasonal and spatial variability of the OM/OC mass ratios and high regional correlation between oxalic acid and zinc in Chinese urban organic aerosols. *Atmospheric Chemistry and Physics*, 13(8), 4307–4318. <https://doi.org/10.5194/acp-13-4307-2013>
- Zhang, J., Huff Hartz, K. E., Pandis, S. N., & Donahue, N. M. (2006). Secondary organic aerosol formation from Limonene Ozonolysis: Heterogeneous and heterogeneous influences as a function of NO_x. *The Journal of Physical Chemistry A*, 110(38), 11053–11063. <https://doi.org/10.1021/jp062836f>
- Zhang, Q., Jimenez, J. L., Canagaratna, M. R., Allan, J. D., Coe, H., Ulbrich, I., et al. (2007). Ubiquity and dominance of oxygenated species in organic aerosols in anthropogenically-influenced Northern Hemisphere midlatitudes. *Geophysical Research Letters*, 34(13), L13801. <https://doi.org/10.1029/2007gl029979>
- Zhang, Q., Xu, Y., & Jia, L. (2019). Secondary organic aerosol formation from OH-initiated oxidation of *m*-xylene: Effects of relative humidity on yield and chemical composition. *Atmospheric Chemistry and Physics*, 19(23), 15007–15021. <https://doi.org/10.5194/acp-19-15007-2019>

- Zhang, X., Cappa, C. D., Jathar, S. H., McVay, R. C., Ensberg, J. J., Kleeman, M. J., & Seinfeld, J. H. (2014). Influence of vapor wall loss in laboratory chambers on yields of secondary organic aerosol. *Proceedings of the National Academy of Sciences*, 111(16), 5802–5807. <https://doi.org/10.1073/pnas.1404727111>
- Zhou, W., Xu, W., Kim, H., Zhang, Q., Fu, P., Worsnop, D. R., & Sun, Y. (2020). A review of aerosol chemistry in Asia: Insights from aerosol mass spectrometer measurements. *Environmental Science: Processes & Impacts*, 22(8), 1616–1653. <https://doi.org/10.1039/d0em00212g>

References From the Supporting Information

- Castro, L. M., Pio, C. A., Harrison, R. M., & Smith, D. J. T. (1999). Carbonaceous aerosol in urban and rural European atmospheres: Estimation of secondary organic carbon concentrations. *Atmospheric Environment*, 33(17), 2771–2781. [https://doi.org/10.1016/s1352-2310\(98\)00331-8](https://doi.org/10.1016/s1352-2310(98)00331-8)
- Huang, C., Wang, H. L., Li, L., Wang, Q., Lu, Q., de Gouw, J. A., et al. (2015). VOC species and emission inventory from vehicles and their SOA formation potentials estimation in Shanghai, China. *Atmospheric Chemistry and Physics*, 15(19), 11081–11096. <https://doi.org/10.5194/acp-15-11081-2015>
- Jeon, H., Park, J., Kim, H., Sung, M., Choi, J., Hong, Y., & Hong, J. (2015). The characteristics of PM_{2.5} concentration and chemical composition of Seoul Metropolitan and inflow background area in Korea peninsula. *Journal of the Korean Society of Urban Environment*, 15(3), 261–271. Retrieved from <https://www.earticle.net/Article/A267061>
- Lim, H.-J., & Turpin, B. J. (2002). Origins of primary and secondary organic aerosol in Atlanta: Results of time-resolved measurements during the Atlanta supersite experiment. *Environmental Science & Technology*, 36(21), 4489–4496. <https://doi.org/10.1021/es0206487>
- Millet, D. B., Donahue, N. M., Pandis, S. N., Polidori, A., Stanier, C. O., Turpin, B. J., & Goldstein, A. H. (2005). Atmospheric volatile organic compound measurements during the Pittsburgh Air Quality Study: Results, interpretation, and quantification of primary and secondary contributions. *Journal of Geophysical Research: Atmospheres*, 110(D7), D07S07. <https://doi.org/10.1029/2004JD004601>
- Pio, C., Cerqueira, M., Harrison, R., Nunes, T., Mirante, F., Alves, C., & Matos, M. (2011). OC/EC ratio observations in Europe: Re-thinking the approach for apportionment between primary and secondary organic carbon. *Atmospheric Environment*, 45, 6121–6132. <https://doi.org/10.1016/j.atmosenv.2011.08.045>
- Wu, C., & Yu, J. Z. (2016). Determination of primary combustion source organic carbon-to-elemental carbon (OC/EC) ratio using ambient OC and EC measurements: Secondary OC-EC correlation minimization method. *Atmospheric Chemistry and Physics*, 16(8), 5453–5465. <https://doi.org/10.5194/acp-16-5453-2016>
- Wu, C., & Yu, J. Z. (2018). Evaluation of linear regression techniques for atmospheric applications: The importance of appropriate weighting. *Atmospheric Measurement Techniques*, 11(2), 1233–1250. <https://doi.org/10.5194/amt-11-1233-2018>
- Yuan, B., Hu, W. W., Shao, M., Wang, M., Chen, W. T., Lu, S. H., et al. (2013). VOC emissions, evolutions and contributions to SOA formation at a receptor site in eastern China. *Atmospheric Chemistry and Physics*, 13(17), 8815–8832. <https://doi.org/10.5194/acp-13-8815-2013>